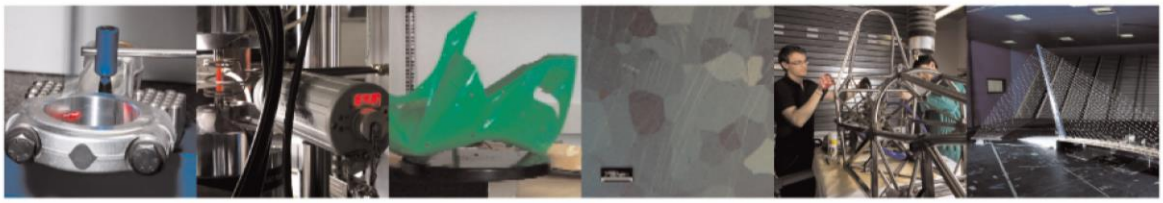

Spatially weighted PCA for monitoring video image data with application to additive manufacturing

Colosimo, Bianca M.; Grasso, Marco

This is an Accepted Manuscript of an article published by Taylor & Francis in JOURNAL OF QUALITY TECHNOLOGY on 31 Oct 2018, available online:
http://dx.doi.org/10.1080/00224065.2018.1507563

DIPARTIMENTO DI MECCANICA ■ POLITECNICO DI MILANO
via G. La Masa, 1 ■ 20156 Milano ■ EMAIL (PEC): pecmecc@cert.polimi.it
http://www.mecc.polimi.it
Rev. 0

Spatially weighted PCA for monitoring video image data with application to additive manufacturing

BIANCA M. COLOSIMO and MARCO GRASSO*

Politecnico di Milano, Via La Masa 1, 20156 Milano, Italy

Abstract. Machine vision systems for in-line process monitoring in advanced manufacturing applications have attracted an increasing interest in the recent years. One major goal is to quickly detect and localize the onset of defects during the process. This implies the use of image-based statistical process monitoring approaches to detect both when and where a defect originated within the part. This study presents a spatio-temporal method based on the Principal Component Analysis (PCA) to characterize and synthetize the information content of image streams for statistical process monitoring. A spatially weighted version of the PCA, called ST-PCA, is proposed to characterize the temporal auto-correlation of pixel intensities over sequential frames of a video-sequence while including the spatial information related to the pixel location within the image. The method is applied to the detection of defects in metal additive manufacturing processes via in-situ high-speed cameras. A k-means clustering-based alarm rule is proposed to provide an identification of defects in both time and space. A comparison analysis based on simulated and real data shows that the proposed approach is faster than competitor methods in detecting the defects. A real case study in Selective Laser Melting (SLM) of complex geometries is presented to demonstrate the performances of the approach and its practical use.

Keywords: image-based process monitoring; in-situ defect detection; k-means clustering; principal component analysis; selective laser melting.

1. Introduction

The use of image data in process monitoring applications has attracted an increasing industrial interest in the recent years (Qiu, 2017). Indeed, the availability of robust, compact and low-cost machine vision systems that are easy to integrate into production plants has considerably increased thanks to continuous technological advances. In addition, high-performance computational capabilities make in-line analysis of image streams and video-

* Prof. Bianca Maria Colosimo (corresponding author) is a full professor in the Department of Mechanical Engineering. Her email is biancamaria.colosimo@polimi.it.

Dr. Marco Grasso is an assistant professor in the Department of Mechanical Engineering. His email address is marcoluigi.grasso@polimi.it.

sequences practically feasible, even in the presence of high spatial and temporal resolutions. In this framework, novel statistical process monitoring (SPM) tools are needed to face big data issues (Megahed and Jones-Farmer, 2015; Qin, 2014), where the term "big" refers both to the complexity of the data format (i.e., video images) and to the high frequency of data acquisition (e.g., up to thousands of frames per seconds).

Megahed et al. (2011) reviewed control charting methods with image data, pointing out that SPM tools can be used not only to monitor the stability of image patterns over time, but also to detect where a change occurred within the image (in terms of location and size). A seminal approach was proposed by Armingol et al. (2003), which consists of designing an individual control chart for each pixel of the image. However, controlling the family-wise Type I error is an issue when a large number of charts (e.g., in the order of thousands and more) are used in parallel. Rather than monitoring the intensity of single pixels, different authors applied traditional SPM methods to monitor synthetic indexes and quality characteristics extracted via image processing algorithms. As an example, various studies applied univariate or multivariate control charts to monitor product dimensions (Horst and Negin, 1992; Tan et al., 1996; Lyu and Chen, 2009), surface properties (Nembhard et al., 2003; Tong et al., 2005; Wang and Tsung, 2005) or other quantities (Liang and Chiou, 2008; Park et al, 2014) measured via in-line machine vision. Other methods (Yan et al., 2015) rely on the use of Principal Component Analysis (PCA) and its multilinear extensions to synthetize the information content of the images. In the framework of hyperspectral images, multivariate-image-analysis (MIA) control charts represent a well-known category of methods that apply the PCA for monitoring purposes (Geladi and Grahn, 1996; Bharati and MacGregor, 1998; MacGregor et al., 2001; Bharati et al., 2003; Yu and MacGregor, 2004; Graham et al., 2007). In MIA, the PCA is separately applied to each image and regions of interest are identified within the "score space" spanned by the image data projections onto the retained principal components (masking operation). Control charts are then applied to synthetic descriptors computed within those regions (e.g., the number of image pixels belonging to the region in Bharati et al., 2003). Both tensor-based PCA and MIA variants for image data were proposed to better capture the overall data correlation structure, which includes temporal, spatial and spectral contributions (Yan et al., 2015; Lu et al., 2008a; Lu et al., 2008b). Their aim consists of avoiding any unfolding operation by applying the analysis to the multi-dimensional data array via higher-order statistics.

All these methods are aimed at detecting a possible change of the image pattern in a sequence of images observed over time. Generally speaking, they focus on the temporal detection of image pattern shifts rather than on the spatial localization of the occurred change within the image. Other authors proposed so-called "spatial control charts" (Megahed et al., 2011), which are applied to one single image at a time to identify the location of defective areas. Jiang and Jiang (1998), Jiang et al. (2005) and Lu and Tsai (2005) applied a univariate control chart to the pixel intensity of the image to localize outlying image regions. This kind of control chart is called "spatial" because the X axis of the chart represents a location on the image, rather than time (Megahed et al, 2011). Spatial control chart methods were studied and extended by Lin and Chiu (2006) and Lin et al. (2007a; 2007b; 2008).

In the presence of textured surfaces, spatial SPM methodologies were proposed by Tunak and Link (2008), Tunak et al. (2009) and Bui and Apley (2017). Another category of methods, a.k.a. anomaly detection (Funck et al., 2003), exploits image segmentation algorithms to isolate defective regions instead of using spatial control charts. These methods were studied by different authors, e.g., Yan et al. (2016), Qiu and Yandell (1997); Qiu (2005); Qiu and Sun (2007); Park et al. (2012), but they belong to image processing rather than SPM.

Spatio-temporal approaches were proposed by Megahed et al. (2012) and He et al. (2016) to detect both the spatial location (and size) of a defect and the change-point in time within the image stream. Megahed et al. (2012) proposed a generalized likelihood ratio (GLR) method based on dividing the image into partially overlapping regions of interest and monitoring the average pixel intensities within them. He et al. (2016) extended this method to multiple fault detection problems.

All the spatio-temporal methods mentioned above focus on SPM for image data, where images are random replicates of an in-control pattern. Compared with the existing literature, our approach has two main novel issues. First, it focuses on SPM for video image data. In this case, videos are not just a sequence of images but they are capturing a dynamic in-control state. As an example, in our proposed case study, dynamic changes are due to a laser melting of a powder bed along a pre-specified trajectory. Thus, the SPM task is evidently more complex, as the out-of-

control state translates into a perturbation of the underlying dynamics. The second element of novelty that, we believe, can have a great potential by itself, is the spatial extension of the PCA for modelling the in-control signature of video image data. In fact, we propose an extension of the so-called T-mode PCA approach (Jolliffe, 2002), called ST-PCA, where a spatial weight matrix is included into the variance-covariance decomposition to describe the spatial contiguity of pixels in each frame of the video sequence. Contrary to other methods mentioned above, this allows performing the eigen-decomposition directly on the spatial correlation matrix of video image data (Stahlschmidt et al. 2015). This ST-PCA is used to model the in-control state of the observed phenomenon and it is combined with a clustering-based alarm rule to detect the local defect onset.

The proposed methodology is applied to a real case study where in-line monitoring of metal additive manufacturing (AM) processes via in-situ high-speed video imaging is of interest. More specifically, we apply the proposed spatio-temporal approach to detect and localize the onset of "hot-spots" within each layer of parts produced via a laser powder bed fusion process (Gibson *et al*., 2010) also known as Selective Laser Melting (SLM). Hot-spot events correspond to local over-heating of the layer caused by out-of-control heat exchanges, which may produce internal and geometrical defects in the final product.

The present study extends previous research on SLM process monitoring (Grasso *et al*., 2017) by proposing a novel spatially weighted T-mode PCA method to enhance hot-spot detection performances.

The remaining part of the work is organized as follows. Section 2 presents the motivating case study in additive manufacturing. Section 3 describes the proposed approach. Section 4 and Section 5 present, respectively, a simulation study and a real case study to determine the performances of the proposed approach. Section 6 concludes the paper.

2. A motivating case study in metal additive manufacturing

Metal AM processes allow producing parts characterized by innovative shapes, complex features and lightweight structures that are difficult or even impossible to produce with conventional systems.

SLM is an AM technology belonging to the category of powder bed fusion processes, where a laser enables the additive production of parts by fully melting a metal powder. A thin powder layer (e.g., thickness of about 30 - 50 μm) is deposited on a baseplate by a powder recoating system. Then, a scanner is used to displace the laser beam along a predefined path and to locally melt the powder to realize the first slice of the part. When the scan of this first layer is complete, the substrate is lowered, a new layer of powder is deposited and the process is repeated to realize the next slice (the interested reader is referred to Gibson *et al*., 2010 for further details). Fig. 1 shows a simple scheme of an SLM system.

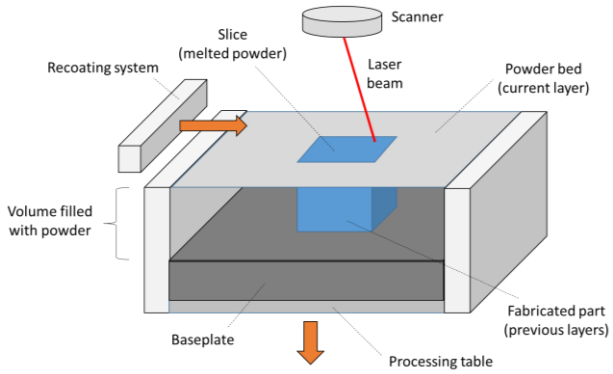

FIGURE 1 – Scheme of the SLM system (building chamber)

Several authors pointed out that the limited stability and repeatability of the process still represent a major barrier to the industrial breakthrough of this technology (Mani *et al*., 2015; Tapia and Elwany, 2014; Everton *et al*., 2016; Spears and Gold, 2016; Grasso and Colosimo, 2017). Indeed, various kinds of defects may originate during the process, with detrimental effects on the quality characteristics of the final product. In this framework, high-speed vision is potentially suitable to characterize fast thermal phenomena related to the laser-material interaction, and to detect the onset of defects. Nevertheless, commercially available systems still lack any automated defect detection capability. An example of an in-situ monitoring setup proposed in Grasso et al. (2017) is shown in Fig. 2a. It consists of an Olympus^{TM} I-speed 3 camera (CMOS sensor) placed outside the build chamber viewport. A sampling frequency of $f = 300$ fps was selected as a compromise between the capability of capturing the laser kinematics without losing relevant information, and the computational feasibility of in-process image analysis.

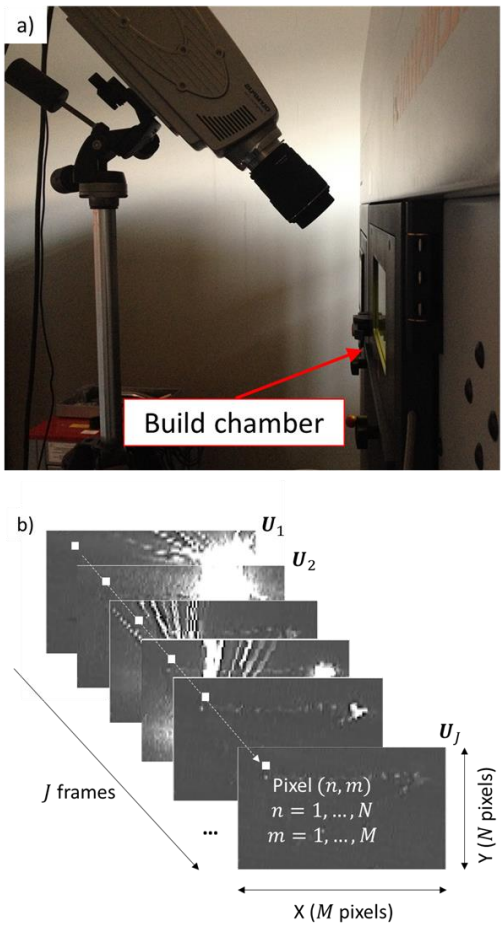

FIGURE 2 – a) Experimental setup for high-speed video imaging on a commercial Renishaw® SLM system (AM250); b) schematic representation of the high-speed image stream

The acquired stream of grey-scale video images (Fig. 2b) can be described in terms of a 3-dimensional array, $\boldsymbol{\mathcal{U}} = \{\boldsymbol{U}_1, \boldsymbol{U}_2, \dots, \boldsymbol{U}_J\} \in \mathbb{R}^{J \times M \times N}$, where $M \times N$ is the size (in pixels) of each frame and J is the total number of acquired frames over a time period of duration $T = J/f$, being f the sampling frequency. $\boldsymbol{U}_j \in \mathbb{R}^{M \times N}$ is the j-th image, $j = 1, \dots, J$, and $\boldsymbol{u}_{n,m} = \{u_{n,m,1}, u_{n,m,2}, \dots, u_{n,m,J}\}$ is the intensity profile of the pixel at location (n, m) over the J acquired frames, with $n = 1, \dots, N$ and $m = 1, \dots, M$.

Grasso et al., 2017 showed that high-speed imaging may be used to detect and localize local "hot-spots" within the scanned slice caused by a wrong heat exchange towards the surrounding material. The loose powder has a lower conductivity than the solid material. Because of this, when laser heated features (e.g., acute corners, overhang zones, thin walls) are largely surrounded by loose powder, the diminished heat flux may yield excessive heat accumulation and slow cooling transitory. This produces an out-of-control solidification mechanism.

Our real case study consists of a complicated shape of about $50 \times 50 \times 50\ mm$ (Fig 3a) produced via SLM of AISI 316L powder (average particle size of about $25 - 30\ \mu m$). Different hot-spot events occurred during the process in correspondence of acute corners belonging to overhang areas shown in Fig. 3b. Fig. 3c shows that these hot-spot events produced local geometrical deformations in the printed part. The major processing parameters are summarized in Table 1. Further details are provided in Grasso et al. (2017).

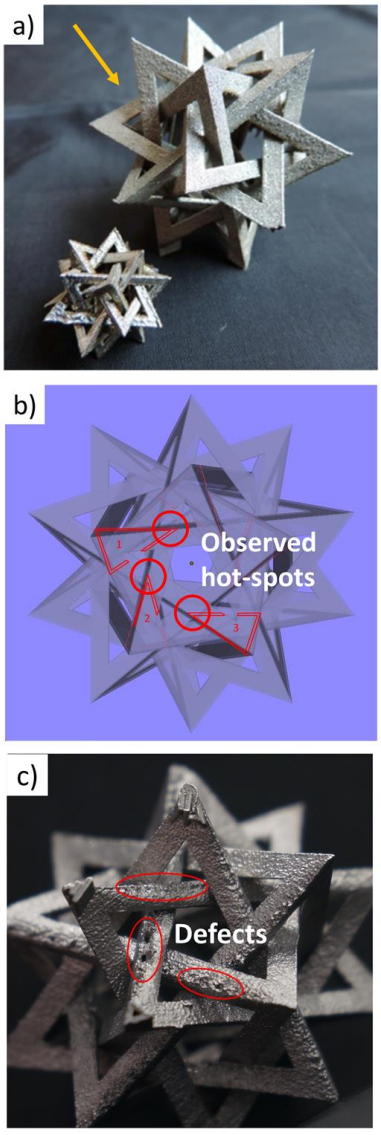

FIGURE 3 – a) complex shape part used to test the proposed approach; b) examples of triangular portions of the sliced CAD model; c) local defects corresponding the acute corners of those triangles.

TABLE 1 – Main process parameters used in the experimental activity

	Power (P)	Exposure time (t)	Focus position (f_p)	Point distance (d_p)	Hatch distance (d_h)	Layer thickness (z)
Value	200 W	80 μs	0 mm	60 μm	110 μm	50 μm

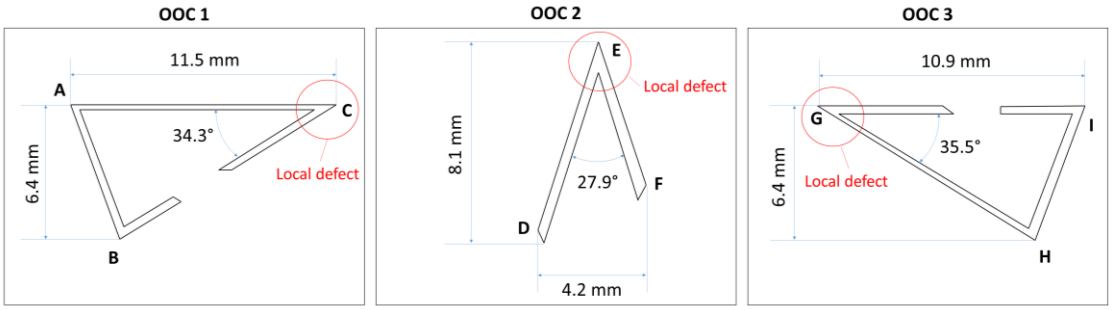

FIGURE 4 – Dimensions of the triangular portions of the part slices monitoring in this study (complex-shape part); the defective corners where over-heating phenomena occurred are highlighted

Three distinct videos were acquired during the SLM of triangular-shaped features in three different layers. Fig. 4 shows these triangular features belonging to the sliced CAD model of the complicated geometry and indicates the acute corners where the hot-spot events occurred. The three corresponding image streams were denoted as OOC scenario 1, 2 and 3, respectively, where OOC stands for "out-of-control".

A checkerboard camera calibration (Zhang, 2000) was performed to estimate the spatial resolution (about 150 µm/pixel). The image acquisition system was set in order to apply a crop operation to remove defocused regions and areas of the baseplate not involved by the process. The resulting image size was 121×71. The maximum number of frames in a video-sequence was 320.

Fig. 5 shows some examples of pixel intensity profiles, $\boldsymbol{u}_{n,m}$ (OOC scenario 1), at different locations of the video frames.

The pixels can be divided into three categories, i.e., i) background pixels (Fig. 5, top panels), belonging to regions where no laser-material interaction occurred, ii) pixels belonging to the normal melting zone (Fig. 5, middle panels), where in-control SLM process occurred, and iii) hot-spot pixels (Fig. 5, bottom panels), where a local out-of-control over-heating occurred. For 8-bit images, the pixel intensity range is $u_{n,m,j} \in [0,255]$, with an average background intensity of about 80. The normal melting zone is characterized by a high cooling rate that leads to a finer grain and stiffer material. The corresponding pixel profiles exhibit frequent spikes corresponding to points in time when the laser heated zone passed over the pixel location. The in-control cooling transitory is very fast, and hence the pixel intensity drops from the saturation level to the background level almost instantaneously. Hot-spot areas, instead, exhibit a saturation level that lasts for a longer time, and the drop from saturation to background intensity is much slower. This is representative of an out-of-control temporal auto-correlation pattern affecting a limited number of adjacent pixel locations.

The in-situ detection and localization of hot-spots is of great industrial importance to achieve zero-defect additive manufacturing capabilities. Indeed, it allows one to stop the process to prevent producing defective parts or, when possible, to implement closed-loop control strategies to mitigate or even repair the defect during the process.

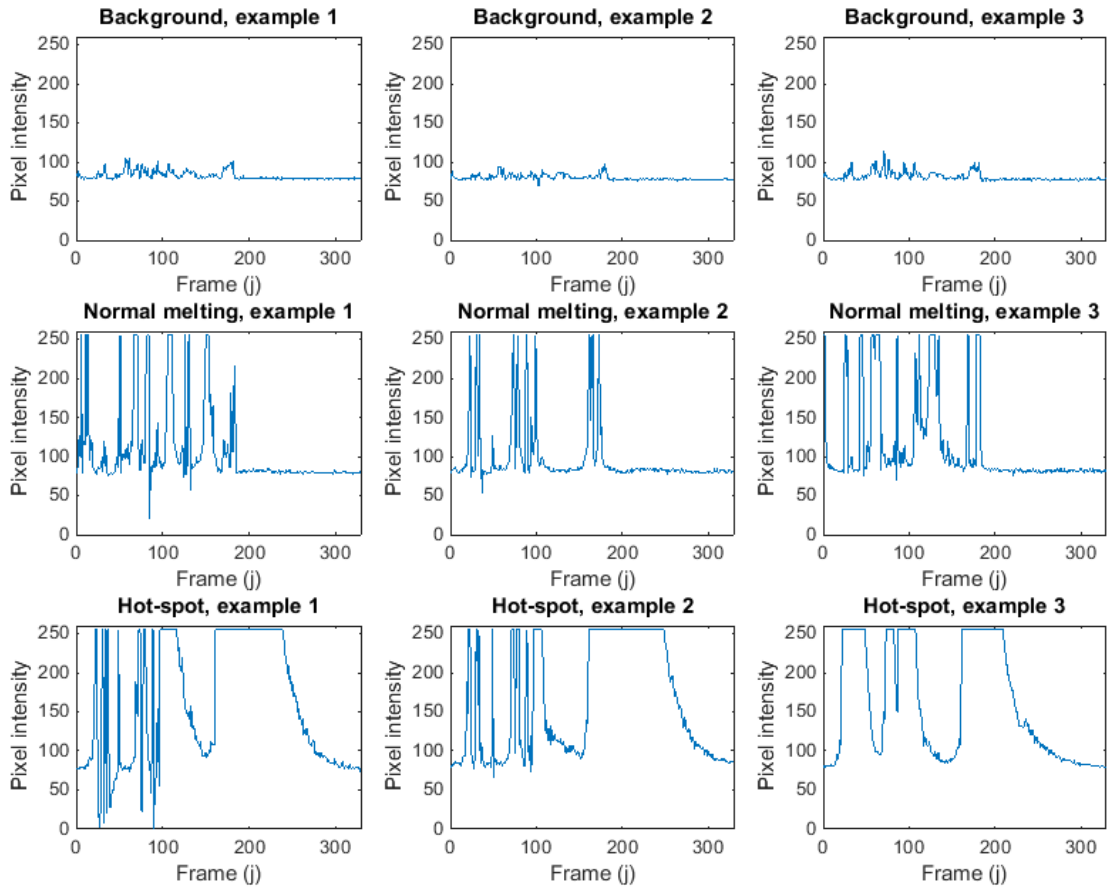

FIGURE 5 – Examples of intensity profiles belonging to background region (top panels), normal-melting zone (middle panels) and an out-of-control hot-spot region (bottom panel)

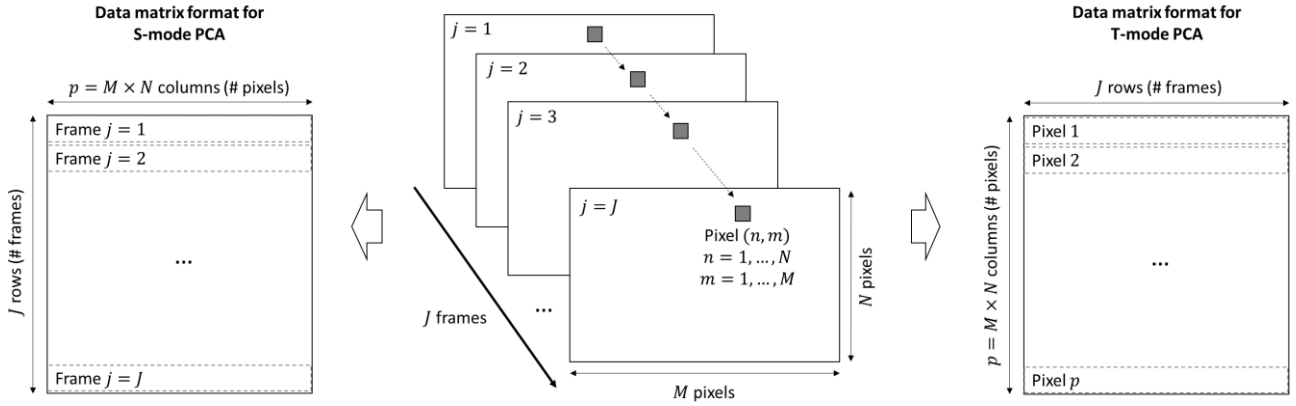

FIGURE 6 – Unfolding of the original image stream into a data matrix for S-mode PCA (left) and T-mode PCA (right)

3. The proposed methodology

Different PCA variants were proposed in the literature to cope with the spatial, temporal or spatio-temporal information content of image data, e.g., in geospatial analysis and atmospheric science (Demsar *et al*., 2013; Compagnucci *et al*., 2001; Jolliffe, 2002). The common approach is known as S-mode PCA (Jolliffe, 2002), where image pixels are treated as variables (columns of the data matrix) and video frames as observations (rows of the data matrix). Therefore, in the S-mode PCA, the 3-dimensional array, $\boldsymbol{\mathcal{U}}$, is converted into a matrix $\mathbf{X} \in \mathbb{R}^{J \times p}$, where $p = M \times N$ (Fig. 6, left side). It is also known as "unfolded" (Yan et al., 2015) or "vectorised" (Grasso et al., 2014) PCA.

The S-mode PCA captures the pixel correlation in space to determine how outlying is each frame with respect to the set of considered images (Compagnucci *et al*., 2001). However, the variation of the image pattern from frame to frame caused by the underlying process dynamics may mask the occurrence of local defects. As a matter of fact, the S-mode PCA approach lacks any spatial localization capability. Tensor-based PCA methods, e.g., the multi-linear PCA and the tensor rank-one decomposition (Yan et al., 2015; Lu et al., 2008a; Lu et al., 2008b) were proposed to overcome this limit. These methods avoid the unfolding operation shown in Fig. 6 by applying an higher-order variant of the PCA to the original multi-dimensional data array, $\boldsymbol{\mathcal{U}}$. The projected low-dimensional tensor captures the most of overall data variability, which includes both spatial and temporal contributions. When applied to image data, these methods yield a synthetic control statistic, e.g., the Hotelling's T^2, that associates one value to each frame. This control statistic allows one to detect when a shift in the video frame sequence has occurred, but not where it is localized within the image. An alternative approach, known as T-mode PCA (Jolliffe, 2002; Tsutsumida et al., 2017), is aimed to achieve a defect spatial localization within the image. It converts the 3-dimensional array, $\boldsymbol{\mathcal{U}}$, into the matrix $\mathbf{X} \in \mathbb{R}^{p \times J}$ (Fig. 6, right side), where the video frames are treated as variables (columns) and image pixels as observations (rows). In particular, the T-mode PCA allows capturing the temporal auto-correlation of pixel intensities over consecutive frames. The projections of the original image data onto the first retained PCs belong to the image space, and hence they let a spatial localization of anomalous regions. Nevertheless, the spatial correlation information is lost, because the actual distance between the pixels of the image is not taken into account. In order to capture both the temporal and spatial auto-correlation of image data, we propose a spatially-weighted version of the T-mode PCA, called ST-PCA. Sub-section 3.1 presents the ST-PCA methodology; sub-section 3.2 describes the methods to iteratively update the ST-PCA model as new frames become available; sub-section 3.3 presents a k-means clustering-based alarm rule suitable for hot-spot detection in SLM process monitoring applications.

3.1. Spatially weighted T-mode PCA (ST-PCA†)

The underlying idea of a spatially weighted T-mode PCA consists of incorporating the pixel spatial correlation into the projection operation entailed by the T-mode PCA. Such spatial information can be incorporated into the PCA by defining a $p \times p$ spatial weight matrix, $\mathbf{W}$. The (k, h)-th element of the matrix, $w_{k,h}$, quantifies the spatial dependency between the k-th and h-th pixels (the higher the value, the higher the dependency).

The use of spatial weights in the basic PCA was proposed by Wartenberg (1985) and Jombart et al. (2008), with applications in geostatistics (Harris et al. 2015). When multivariate spatial data are monitored over time, Stahlschmidt *et al*. (2015) extended those methods and proposed computing a time average of the spatially weighted covariance matrices associated to different points in time, and applying an eigen-decomposition of this average. Differently from the approach of Stahlschmidt *et al*. (2015), we introduce the spatial weights into the T-mode PCA formulation, where different points in time (i.e., the frames) are treated as variables, and the eigen-decomposition applies to the T-mode covariance matrix that already encloses the temporal auto-correlation information.

The proposed ST-PCA works by applying the spectral decomposition to the weighted sample variance-covariance matrix defined as $\mathbf{S} = \frac{1}{p-1}(\mathbf{X} - \mathbf{1}\bar{\mathbf{x}})^T \mathbf{W} (\mathbf{X} - \mathbf{1}\bar{\mathbf{x}})$, where $\mathbf{X} \in \mathbb{R}^{p \times J}$ is the data matrix of the T-mode PCA formulation (Fig. 6, right side) ,

† The ST-PCA nomenclature should not be confused with the stPCA proposed by Stahlschmidt *et al*., 2015, where more than one variable is measured at different locations, and a time-averaged spatial covariance matrix is considered.

$\bar{\mathbf{x}} \in \mathbb{R}^{1\times J}$ is the sample mean vector and $\mathbf{1}$ is a $p \times 1$ vector of ones.

The matrix $\mathbf{S}$ is a quadratic form whose decomposition into orthogonal components via eigenvector analysis has a closed analytical solution, being $\mathbf{W}$ a symmetric weighting matrix (Koren and Carmel, 2004). This allows projecting the image data onto a new coordinate system while preserving the spatial correlation between the locations. The i-th loading, $\boldsymbol{v}_i \in \mathbb{R}^J$, $i = 1, \dots, p$, is a vector of length J that associates a temporal weight to each frame. Thus, each PC is a linear combination of points in time (i.e., the frames). The j-th score, $\boldsymbol{z}_j \in \mathbb{R}^{M\times N}$, $j = 1, \dots, J$, is a matrix of the same size of the original images, and hence it encloses the spatial information associated to each PC. The selection of the number, $m < J$, of most relevant PCs follows the same principle of the traditional PCA (Jolliffe, 2002). In particular, m can be selected by setting a threshold on the cumulative variance explained by the retained PCs. This simple approach allows comparing in a fair way different PCA-based methods being equal the percentage of the explained variance.

Three different spatial weight definitions were considered and compared in this study, indicated by the matrices W_1, W_2 and W_3, and defined as follows:

$$
\begin{aligned}
&W_1: \{w_{i,j} = 1/d_{i,j}^2\} \\
&W_2: \{w_{i,j} = 1 \; if \; d_{i,j} \le r, w_{i,j} \\
&\qquad\qquad = 0 \; otherwise\} \\
&W_3: \{w_{i,j} = (1 - d_{i,j}/r^2)^2 \; if \; d_{i,j} \le r, w_{i,j} \\
&\qquad\qquad = 0 \; otherwise\}
\end{aligned}
\qquad (1)
$$

where $d_{i,j}$ is the Euclidean distance between the i-th and j-th pixels of the image, and r is a reference distance threshold. The weight definitions in W_2 and W_3 are also known an box-car and bi-square kernel functions, respectively (Harris *et al*., 2014, 2015). They are discontinuous functions commonly used in geographically weighted models (Harris *et al*., 2011; Harris *et al*., 2014; Gollini *et al*., 2015; Demsar *et al*., 2012), which set weights to zero at distances longer than r (in this study, $r = 5$). The weight definition in W_1 involves a continuous weight decrease proportional to the square of the inter-pixel distance. The bi-square kernel (W_3) couples a decaying weight formulation with a discontinuity at the pre-defined value r. The elements on the main diagonal of $\mathbf{W}$ are set to zero ($w_{k,k} = 0$) and the weights, $w_{k,h}$, are scaled to sum to 1 (Wartenberg, 1985). In the rest of the paper, the term ST-PCA(W_i) will be used to denote the adoption of the i-th spatial weight matrix formulation defined in Equation 1.

It is worth noticing that introducing a spatial weighting into the eigen-decomposition entailed by the ST-PCA can be regarded as a special case of kernel PCA (Scholkopf et al., 1997) where the kernel-based transformation is aimed at capturing the spatial closeness of pixels within the image.

In this study, we propose using the Hotelling's T^2 statistic just as a synthetic index to describe the information content along the most relevant components of the image data within the J acquired frames. The adoption of the T^2 statistic to synthetize the information is similar to the approach proposed by Lin and Chiu (2006), although we envisage a different PCA formulation and use. Analogously to the T-mode formulation, this statistic is such that $T_i^2 \in \mathbb{R}^{M\times N}$, $i = 1, \dots, p$ and it is defined as follows:

$$
T^2(m,n) = T_i^2 = \sum_{j=1}^{m} \frac{z_{j,i}^2}{\lambda_j}, \qquad i = 1, \dots, p \qquad (2)
$$

where λ_j is the j-th eigenvalue and (m, n) are the i-th pixel coordinates. The $T^2(m,n)$ associates one T^2 value to each pixel location. Areas of the image characterized by different temporal auto-correlation patterns will result in different levels of the $T^2(m,n)$ statistic. This provides a capability of locating anomalous patterns that exploits both the temporal and spatial dependencies in the image stream. Moreover, contrary to the T-mode PCA, every possible arrangement of the image pixels in one row of the $\mathbf{X}$ matrix yields the same spatial pattern of the $T^2(m,n)$, thanks to the enclosure of the spatial correlation information into the statistic estimation.

3.2. Iterative updating

In order to combine the spatial defect localization with the ability to monitor the stability of the process over time, the ST-PCA must be iteratively updated as new frames (or batches of frames) become available. Recursive and moving window PCA updating schemes were proposed to cope with non-stationary process patterns (De Ketelaere *et al*., 2015). However, they are usually combined with the traditional (S-mode) PCA implementation. In this section, we briefly review their application to the ST-PCA.

The recursive updating approach was originally proposed by Wold (1994) and Gallagher *et al*. (1997), and a computationally efficient algorithm was proposed by Li *et al*. (2000). The underlying idea consists of augmenting the data matrix by including

any new observation, unless an out-of-control state is detected, and the PCA model and the control chart parameters are updated accordingly. In the ST-PCA framework, let $\mathbf{X}_{1:p,1:j}$ be the data matrix that includes j frames (columns). When a new frame becomes available, the data matrix is augmented to $\mathbf{X}_{1:p,1:j+1}$ and an ST-PCA model based on this data-matrix is computed. If the pattern of the resulting synthetic statistic, $T^2(m,n)$, is judged in-control (see sub-section 3.3 for a discussion on the alarm rule), the procedure is repeated for the following frame, otherwise an alarm is signalled. Thus, differently from the traditional recursive approach, the number of columns is iteratively updated instead of the number of rows. A schematic representation of this approach is shown in Fig. 7a.

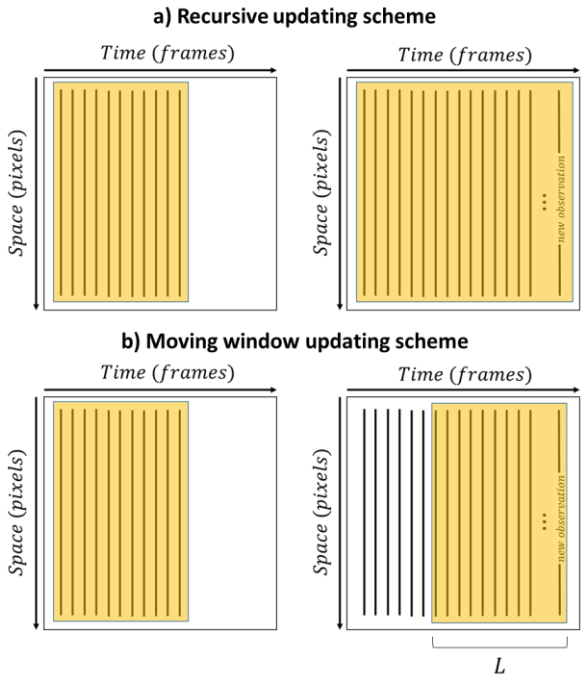

FIGURE 7 – Schematic representation of a recursive (a) and moving window (b) updating scheme combined with the ST-PCA

The moving window updating approach works by restricting the observations used in the estimation of the PCA model to those included into a window of most recent acquisitions (Wang *et al.*, 2005; De Ketelaere *et al.*, 2015). The underlying idea consists of iteratively augmenting the data matrix by including the new observation and by discarding the oldest one, keeping fixed the size, L, of the moving window. In the ST-PCA framework, let $\mathbf{X}_{1:p,j-L+1:j}$ be the data matrix that includes the L most recent frames (columns). When a new frame becomes available, the moving window is shifted such that the ST-PCA is applied to $\mathbf{X}_{1:p,j-L+2:j+1}$. If the pattern of the synthetic $T^2(m,n)$ statistic is judged in-control, the procedure is repeated for the next frame, otherwise an alarm is signalled. A schematic representation of this approach is shown in Fig. 7b.

Both the recursive and the moving window approach can be applied either to update the ST-PCA for each new frame or for a batch of newly acquired frames. The latter solution may be more convenient to cope with real-time computational constraints in the presence of high-speed videos. However, the larger is the size of the batch, the larger will be the delay in detecting a possible out-of-control state, as in the use of batching for traditional control charts. The advantage of the moving window updating scheme consists of keeping constant the computational cost during the entire process, but its performances may depend on the selection of the window length, L. In this study, we compare the two methods combined with the ST-PCA and we provide some advices to the practitioner on their practical use in Section 5.

As far as the basic (or S-mode) PCA formulation is concerned, some authors proposed computationally efficient algorithms to recursively update the eigen-decomposition. As an example, Li et al. (2000) introduced a recursive PCA update based on rank-one modification and Lanczos tridiagonalization, whereas Wang et al. (2005) proposed the so-called fast moving window PCA. These methods are applicable to the S-mode PCA, where the number of variables (i.e., the pixels) is kept constant, and the number of observations (i.e., the acquired frames) grows over time. Their extension to the T-mode PCA, where the number of variables (i.e., the acquired frames) grows over time, is more challenging and requires further research developments, although it represents a relevant issue to enable a faster and more efficient real-time implementation of T-mode and ST-PCA methodologies.

3.3. K-means clustering-based alarm rule

In this sub-section, we briefly review an automated alarm rule based on spatial clustering that encloses engineering knowledge about the SLM process. For more details, we refer the interested reader to Grasso *et al.* (2017).

The alarm rule is aimed at automatically detecting and localizing the existence of hot-spots in the $T^2(m,n)$ pattern. The k-means algorithm represents an effective and popular technique to segment a dataset into k groups characterized by maximum within

similarity (Hastie *et al*., 2009). In this case, the k-means algorithm is applied to the $T^2(m,n)$ spatial pattern by relying on the following assumption: under in-control conditions, only two clusters are expected, one corresponding to background pixels and one corresponding to the normal melting area (as discussed in Section 2). In the presence of a hot-spot, an additional cluster is expected, as a symptom of an out-of-control state. Therefore, the k-means clustering is applied to the $T^2(m,n)$ values by iteratively setting an increasing number k of clusters. A so-called "cluster validity" criterion is applied to automatically select the "correct" number of clusters that better explain the data partition (Zhao et al. 2009; Hastie et al. 2009). Then, the monitoring statistic simply consists of the number of clusters, k, that, accordingly to the aforementioned criterion, better fits the $T^2(m,n)$ pattern. If $k = 2$ the process is judged in-control, otherwise, when $k > 2$, an alarm is signalled. Despite being an "unconventional" SPM approach, such clustering-based alarm rule exploit engineering knowledge about the SLM process. Indeed, the in-control and out-of-control number of clusters have a physical interpretation from the production process viewpoint, and this interpretation allows designing an alarm rule for SLM processes whose dynamics may continuously change from layer to layer (depending on the geometry of the part) and from part to part (e.g., in the presence of customized and one-of-a-kind products).

A method for the selection of the number k consists of looking for an elbow point in the sums of squared within-distances (SSWs) of the $T^2(m,n)$ values of pixels belonging to each cluster and their mean value in the cluster, for different numbers k. The $SSW(k)$ index is computed as follows:

$$SSW(k) = (1/k)\sum_{l=1}^{k}\sum_{(m,n)\in c_l}\left(T^2(m,n)_{c_l} - \overline{T^2}_{c_l}\right)^2, \quad k = 1,2,\ldots \tag{3}$$

where $T^2(m,n)_{c_l}$ is the T^2 value of the (m,n)-th pixel belonging to the c_l cluster and $\overline{T^2}_{c_l}$ is the mean T^2 value of the corresponding cluster. $SSW(k)$ is a monotone decreasing function of the number of clusters k, and its elbow identifies the number k such that a further partition does not significantly improve the clustering result. The $SSW(k)$ index is divided by k in order to penalize the so-called "over-segmentation", i.e., the selection of too many clusters. This penalization is driven by the knowledge that only two clusters are sufficient to characterize the in-control pattern.

It is worth noticing that the $SSW(2)$, i.e., the SSW statistic estimated when $k = 2$ clusters are assumed to be present, may represent by itself a control statistic for alarm rule development. Indeed, the larger is $SSW(2)$, the higher is the probability that more than two clusters exist. Nevertheless, the estimation of a control limit for this statistic can be challenging in practice, due to the lack of an actual training phase, as the process dynamics continuously change. Anyway, future analysis may be envisaged to address this possible variant of the proposed method.

4. Simulation analysis

In order to investigate the benefits of including the spatial correlation information into the T-mode PCA formulation, a simulation analysis was carried out by artificially injecting hot-spot events of different duration and size into a real image stream. The reference high-speed video used for this analysis is a 150 fps video-sequence acquired during the SLM of a cylindrical shape of diameter $\emptyset = 16$ mm. The video-sequence was acquired during the realization of one layer by using the setup shown in Fig. 8 (see Section 5 for details on the experimentation).

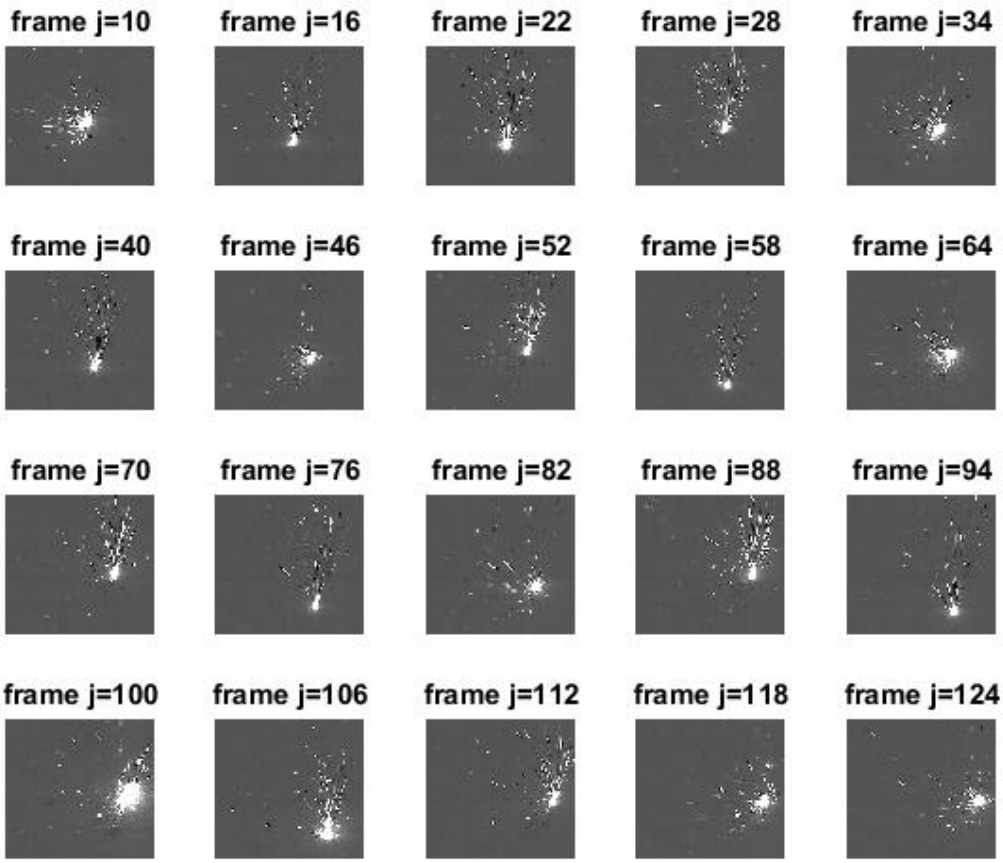

FIGURE 8 – Examples of video frames during the SLM of a cylindrical part

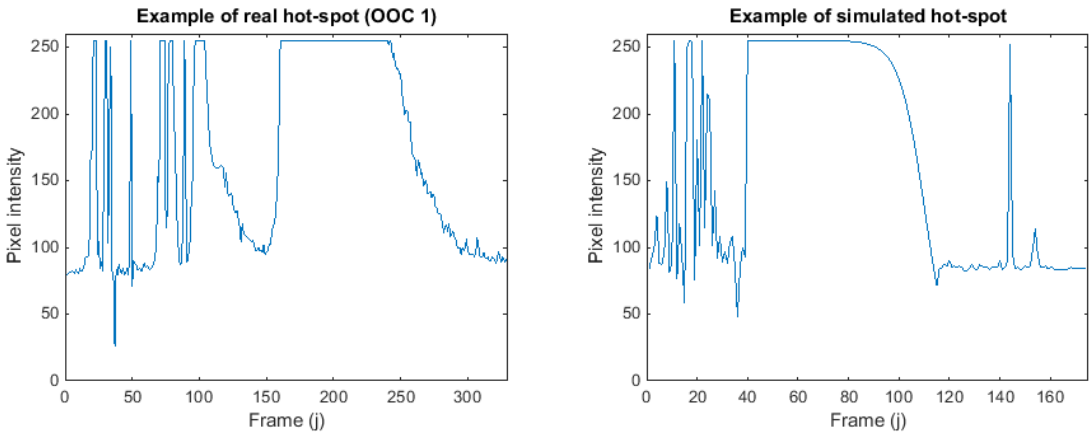

FIGURE 9 – Example of pixel-intensity times series in the presence of a real hot-spot in OOC scenario 1 (left panel) and example of pixel-intensity time series with simulate hot-spot of duration $\tau = 75$ (right panel)

Fig. 8 shows an example of a subset of video frames, before injecting the hot-spot. This image stream is representative of an in-control process, where no anomalous behaviour was observed, the final quality of the part was acceptable and all the considered competitor techniques yielded no alarm.

Hot-spot events were simulated by modifying the pixel intensity of a number n of adjacent pixels for a

given duration, τ. Three levels of hot-spot size were considered, corresponding to $n = 9$ (small), $n = 20$ (medium) and $n = 45$ (large).

The hot-spot consists of a saturated intensity ($u_{m,n,j} = 255$) for several consecutive frames followed by a slow cooling transitory (i.e., a pixel intensity decrease) to the average background intensity. A sigmoid function was used to generate this pattern, accordingly to the following expression:

$$u_{m,n,j}(\tau) = 255/(1 + \exp(0.2(j - 0.95\tau)), \quad j = 1, \dots, \tau \quad (4)$$

Expression (4) generates a realistic hot-spot pattern over time. As an example, Fig. 9 (right panel) shows a pixel-intensity time-series pattern with a simulated hot-spot of duration $\tau = 75$ frames, compared with a pattern produced by a real hot-spot in OOC scenario 1 (Fig. 9, left panel).

Fig. 10 shows three examples of a single frame where the hot-spot was injected at three different sizes. Cross-shaped hot-spots were simulated at medium and large sizes to make them more easily visible in the figures also when displayed in black and white. Anyway, we observed that the shape of the hot-spot does not affect the results of the analysis.

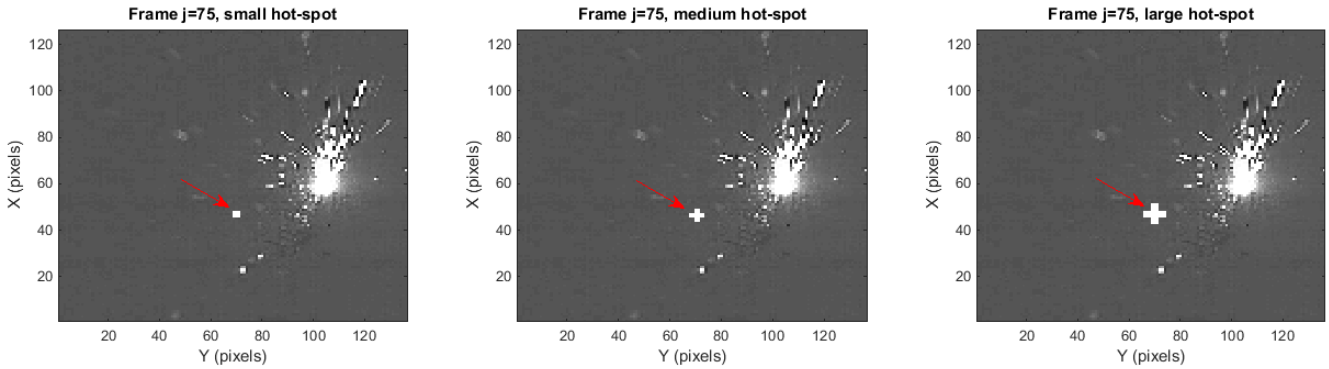

FIGURE 10 – Examples of one single frame where an hot-spot event of different sizes were injected (arrows indicate the spatial location of the hot-spot)

Hot-spot events were randomly injected in 100 different locations of the image, starting from the 51st frame. For each hot-spot location and size, the duration τ was varied in the range $\tau \in [1, 180]$.

Sub-section 4.1 first presents a discussion on the performances of a tensor-based PCA approach applied to this simulation study. Sub-section 4.2 presents a more in-depth comparison between the hot-spot detection performances provided by the T-mode PCA and the ST-PCA.

4.1. A comparison against tensor-based PCA

The multilinear PCA proposed by Lu et al., (2008a) was used in this study as representative of tensor-based PCA methodologies that allow extending the S-mode PCA by capturing both spatial and temporal information. It works by determining a multilinear transformation that maps the original tensor space $\mathbb{R}^{M \times N \times J}$ into a tensor subspace $\mathbb{R}^{P_1 \times P_2 \times J}$ with $P_1 < M$ and $P_2 < N$, where M and N are the dimensions of the video frames. P_1 and P_2 are the number of PCs retained to capture a given percentage of data variability along the "first mode" (size M) and "second mode" (size N) of the original data tensor. For a detailed description of the method we refer the reader to Lu et al., (2008a). An approximate approach for dimensionality reduction consists of truncating the first and second mode eigenvectors beyond the $(P_1)^{th}$ and $(P_2)^{th}$such that the retained fraction of the data variability in each mode is equal to a given percentage. This method is an extension of the dimensionality reduction strategy of the regular PCA to the multi-linear case (Grasso et al., 2014). The Hotelling's T^2 statistics can then be use to synthetize the information content along the retained PCs. This statistic associates one value to each frame, and hence the alarm rule described in Section 3 is not applicable. A more traditional T^2 control chart can be designed instead. The following approach was used in this study: the first K frames of the current in-control

video-sequence were used to estimate the multilinear PCA parameters and to design the T^2 control chart[‡] with empirical control limit (by default we set the Type I error $\alpha = 0.0027$). Then, either the recursive or moving window schemes were applied to update the multilinear PCA model and the control limit estimation as new frames deemed in-control were acquired. We set $K = 50$ frames to initiate the control chart design, because hot-spot injection always started at the 51st frame in our simulation analysis. The T-mode PCA and the ST-PCA were coupled with the clustering-based alarm rule described in Section 3, by using either a recursive or a moving window updating scheme. In the latter case, for all the tested methods, a window size $L = 50$ was applied. Too small window sizes may compromise the capability of capturing the intrinsic behaviour of the process, but, on the other hand, too large window sizes may reduce the computational benefit with respect to the recursive updating scheme. In the present analysis, $L = 50$ was selected as a reasonable compromise between these two issues. However, a sensitivity analysis was carried out and its results are discussed in Section 5.

In order to guarantee a fair comparison between the competitor approaches, the number of retained PCs, m, for the estimation of the Hotelling's statistic was selected by setting the same threshold on the percentage of expected variance. It was observed that, especially in the simple T-mode PCA, the number of PCs to explain even 50% of the overall variability was quite large. Thus, comparisons were made by considering two levels of explained percentage, one at 50% and a more conservative one at 80%. In the multilinear PCA, the same threshold was applied on the variability explained in both the modes (Grasso et al., 2014).

Table 2 shows the performances of the competing methods when applied to the in-control video sequence, where no hot-spot injection was applied. The approaches based on the T-mode and the ST-PCA (coupled with any spatial weight matrix defined in Section 3) yielded no alarm, whereas the multilinear PCA-based approach issued alarms with both the recursive and the moving window updating methods. As an example, Fig. 11 shows the multilinear PCA-based control charts with explained variance threshold at 50% where the first alarm was issues at frame $j = 79$ in recursive updating mode (left panel) and at frame $j = 100$ in moving window updating mode (right panel).

TABLE 2 – Performances of the competitor methods in the presence of the in-control video-sequence

Update approach	% explained variance	Run Length (# frames)		
		Multilinear PCA	T-mode PCA	ST-PCA
Recursive	50%	79	No alarm	No alarm
	80%	84	No alarm	No alarm
Moving window ($L = 50$)	50%	100	No alarm	No alarm
	80%	100	No alarm	No alarm

The result in Table 2 highlights the lower robustness of the multilinear PCA-based approach to the natural frame-to-frame variability caused by the SLM process dynamic. In order to compare the three methods being equal the in-control performances, the type I error, α, used in the multilinear PCA-based control chart was iteratively reduced until no alarm was issued in the in-control video-sequence. This yielded to $\alpha < 0.0001$ in all the considered implementations. Then, the multilinear PCA-based control chart was applied to the out-of-control scenarios. The result was that no alarm was issued at any hot-spot severity level. This further result highlights the lower sensitivity of the multilinear PCA-based method to local out-of-control events that affect a very limited region of the frame. Indeed, the natural process dynamic tends to mask the occurrence of local out-of-controls, which reduces the effectiveness of traditional monitoring tools.

[‡] Notice that it is a common practise to monitor not only the T^2 statistic, but also the sum of prediction errors along directions orthogonal to the retained ones; however, for a fair comparison against the T-mode PCA and ST-PCA based approaches, only the T^2 control chart was considered for the multilinear PCA too.

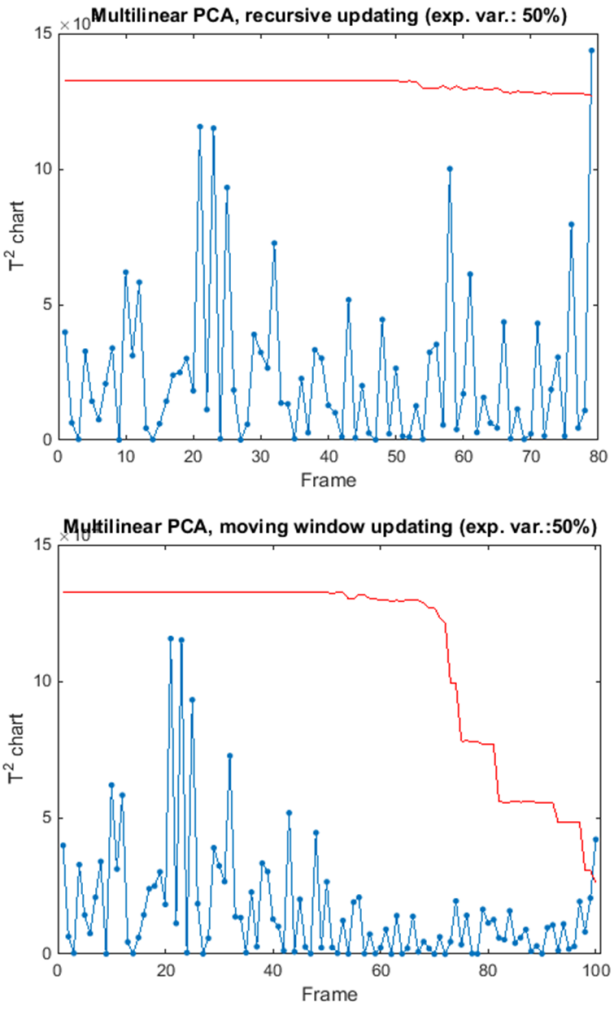

FIGURE 11 – Examples of T^2 control charts based on multilinear PCA applied to the in-control video-sequence (left panel: recursive update, 50% explained variance; right panel: moving window update, $L = 50$, 50% explained variance)

4.2. Comparison between T-mode PCA and ST-PCA

Fig. 12 shows the number of PCs for the T-mode PCA and the ST-PCA(W_1)[§] corresponding to 50% and 80% of explained variability, when the analysis was applied to the original video (no hot-spot).

Fig. 12 shows that the ST-PCA is always more efficient than the T-mode PCA in terms of number of PCs needed to explain a given percentage of variance. In the T-mode PCA, at the end of the process, more than 50 PCs are needed to explain about 50% of the overall variability, whereas in the ST-PCA slightly more than 10 PCs are sufficient to capture 80% of the variability. This is a first major advantage of the ST-PCA formulation against the basic T-mode PCA. Fig. 12 also shows that the moving window updating scheme allows avoiding a continuous increase of the number of retained PCs, m, because the PCA always applies to a batch of frames of fixed dimension, with consequent benefits in terms of computational costs.

Fig. 13 and Fig. 14 show two examples of a comparison of k-means clustering results when the explained variance threshold is set at 50% and the two different updating schemes are used. Both Fig. 13 and Fig. 14 refer to a simulation run where the hot-spot centroid was located approximately at pixel coordinates $X = 70$ and $Y = 40$, for different values of τ (i.e, the τ corresponding to a first signal from the ST-PCA based approach).

The closeness of the hot-spot to the normal melting zone is representative of real conditions, as the hot-spot originates just after the transition of the laser spot over the critical area. Fig. 13 compares the k-means clustering results for the T-mode PCA and the ST-PCA(W_1) when the recursive updating scheme was used. The black area corresponds to the cluster of background pixels, the grey area to the "normal melting" cluster and the red area to the "hot-spot" cluster. Fig. 13 shows that, for the considered values of τ, only the ST-PCA(W_1) allows signalling and localizing the hot-spot. This is made possible thanks to a wider gap between the $T^2(m,n)$ values in the hot-spot region and the ones in the normal melting region. Indeed, the inclusion of the spatial correlation information enhances the identification of regions of adjacent clusters that exhibit anomalous intensity patterns.

Fig. 14 compares the k-means clustering results for the T-mode PCA and the ST-PCA(W_1) when the moving window updating scheme was used with $L = 50$. In this case, the T-mode PCA allows detecting only the medium and large size hot-spots. This confirms the enhanced power of the ST-PCA to anticipate the detection of this kind of events.

The general results of the simulation analysis are shown in Fig. 15 and summarized in Table 3. The T-mode PCA and the ST-PCA were compared by using

[§] Other definitions of the weight matrices for the use in the ST-PCA yielded very similar numbers of retained PCs.

as performance indicator the average run length (ARL), expressed in number of frames. For sake of clarity, Fig. 15 shows a comparison of the 95% confidence intervals of the ARL for the T-mode PCA and ST-PCA(W_1) only, when the first m PCs explain at least 50% of the overall variability. The complete results are shown in Table 3.

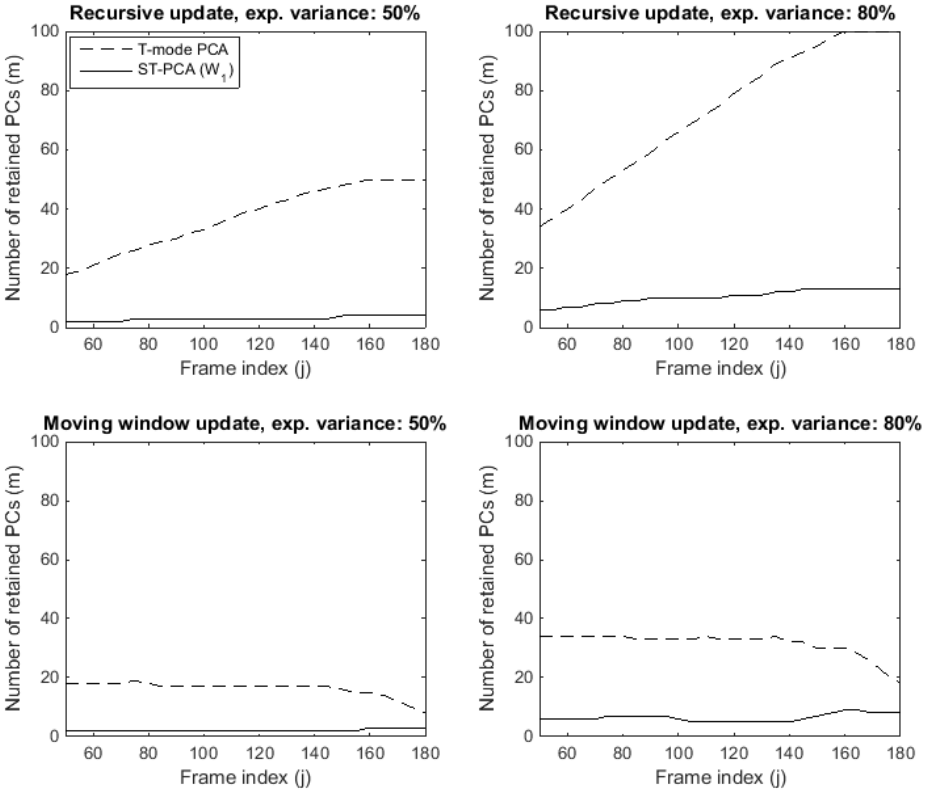

FIGURE 12 – Comparisons between the number of PCs retained by using the T-mode or the ST-PCA (W_1) for different levels of explained variance and different iterative updating methods

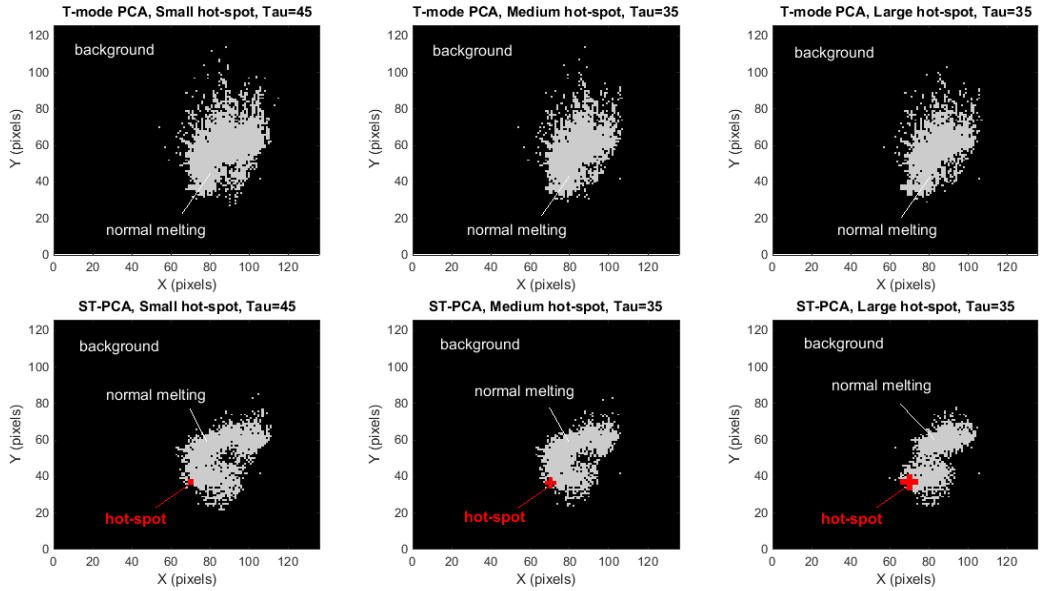

FIGURE 13 – Comparison of k-means clustering results for the T-mode and ST-PCA (W_1) based methods – recursive updating scheme and explained variance threshold at 50%

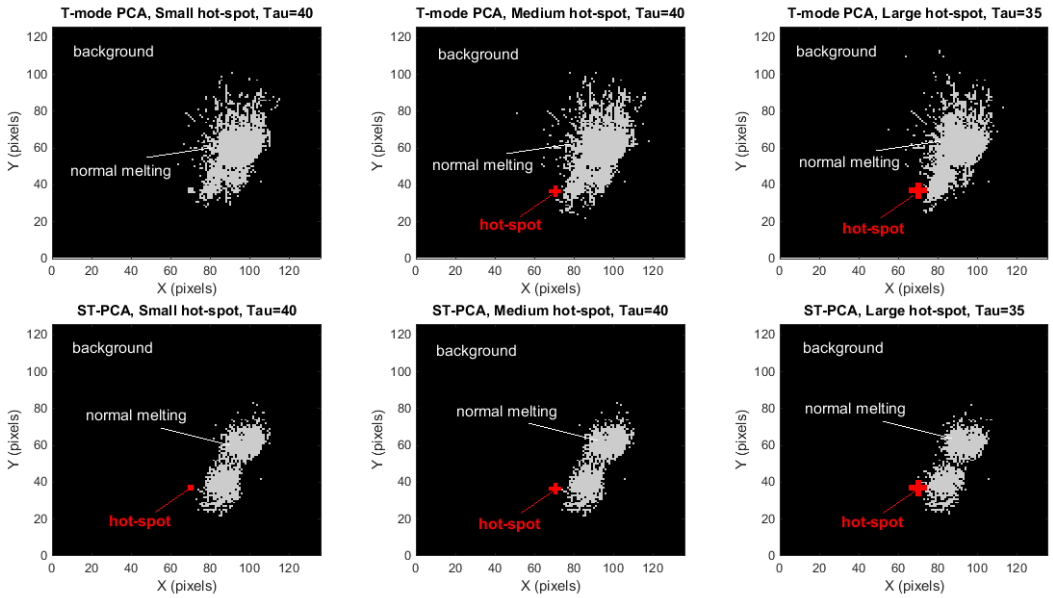

FIGURE 14 – Comparison of k-means clustering results for the T-mode and ST-PCA(W_1) based methods – moving window ($L = 50$) updating scheme and explained variance threshold at 50%

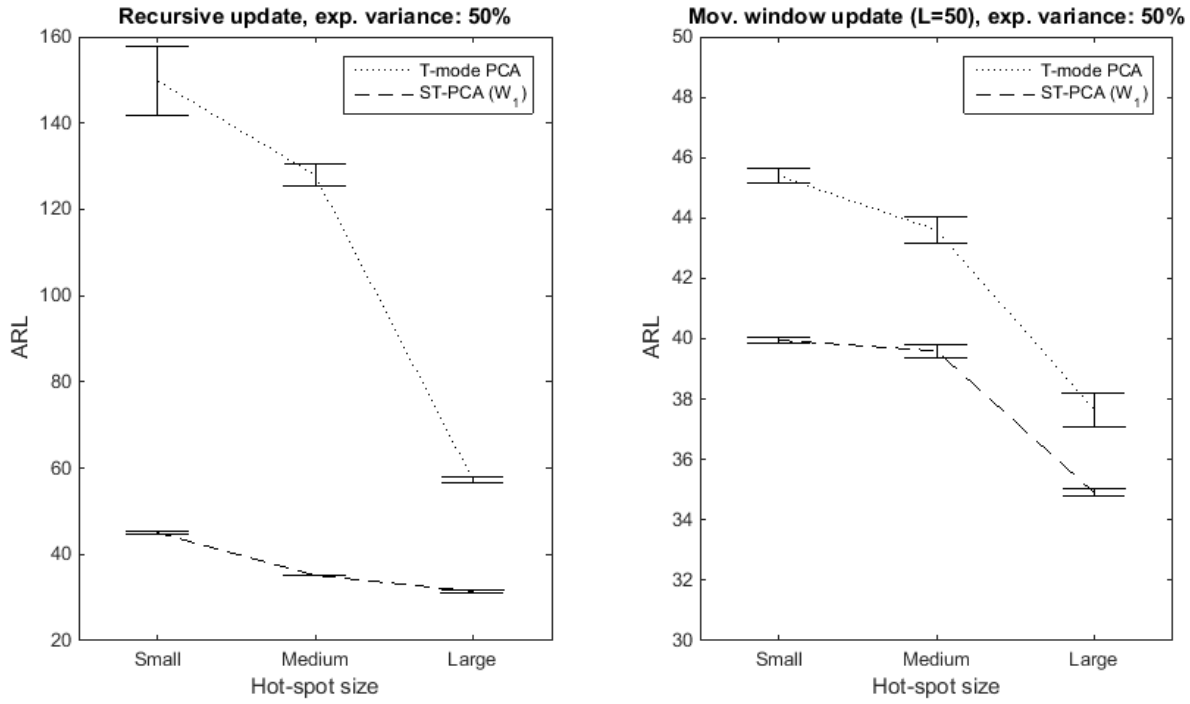

FIGURE 15 – 95% confidence intervals of the ARL for the T-mode and ST-PCA-based methods; results obtained by applying the recursive updating scheme (left panel) and the moving window updating scheme (right panel)

TABLE 3 – Summary of simulation analysis results (bold fonts indicate the best performances in terms of ARL)

Update approach	% explained variance	Hot-spot size	ARL (# frames)			
			T-mode PCA	ST-PCA (W_1)	ST-PCA (W_2)	ST-PCA (W_3)
Recursive	50%	Small	149.79 (47.94)	**45 (1.74)**	45.05 (1.81)	45.05 (1.81)
		Medium	127.90 (14.86)	35.15 (0.86)	**34.80 (1.32)**	**34.80 (1.41)**
		Large	57.30 (4.44)	31.45 (2.39)	**26.95 (2.74)**	**26.75 (2.60)**
	80%	Small	No alarm	122.02 (3.34)	**115.50 (5.48)**	116.60 (6.89)
		Medium	No alarm	**49.90 (15.14)**	50.95 (12.65)	52.20 (12.38)
		Large	No alarm	**38.10 (8.22)**	39.05 (8.70)	39.85 (9.57)
Moving window ($L = 50$)	50%	Small	45.40 (1.54)	**39.95 (0.50)**	**39.95 (0.50)**	**39.95 (0.50)**
		Medium	43.60 (2.57)	**39.60 (1.36)**	**39.60 (1.36)**	**39.60 (1.36)**
		Large	37.65 (3.29)	**34.90 (0.70)**	**34.90 (0.70)**	**34.90 (0.70)**
	80%	Small	No alarm	No alarm	No alarm	No alarm
		Medium	No alarm	**38.70 (9.79)**	47.40 (8.57)	47.10 (11.64)
		Large	No alarm	**35.75 (3.65)**	37.05 (6.56)	37.15 (7.12)

As expected, the larger is the size of the hot-spot, the faster is its detection with both the compared methods. However, Fig. 15 shows that the ST-PCA-based approach allows anticipating the defect detection with respect to the T-mode based approach, by using both a recursive or a moving window updating. As far as the recursive update is concerned, the T-mode based approach requires a longer time to signal the hot-spot (more than 120 frames in the presence of a small or medium hot-spot), whereas the ST-PCA-based approach always signals the out-of-control condition with ARL< 50 frames. This is caused by the fact that the T-mode PCA is less efficient in terms of dimensionality reduction and only a small number of first T-mode PCs are affected by the hot-spot. Therefore, the hot-spot effect on the $T^2(m,n)$ statistic is mitigated by the presence of a large number of unaffected PCs. In the ST-PCA, instead, a lower number of PCs is retained, and the presence of the hot-spot affects most of them, which is a consequence of making a better use of the spatial auto-correlation information. This yields a faster detection, even when the size of the hot-spot is small.

The performances of the T-mode improved by using a moving window updating scheme. This is caused by two reasons: first, the number of retained PCs is much lower than in the recursive case and it does not grow over time, which reduces the mitigation effect caused by the several PCs not affected by the hot-spot. Second, by discarding older frames where no hot-spot was present, it is possible to inflate the effect of the hot-spot itself. This effect becomes maximum when the hot-spot affects all the frames included into the time window. Therefore, the hot-spot can be either detected within a maximum time period equal to the window size (i.e., ARL$\leq L$), or not detected at all. Table 3 shows that the T-mode based approach allows detecting the hot-spot only by setting the threshold of explained variance for the selection of m at 50%. When the threshold is set at 80%, the T-mode PCA never yields an alarm. Indeed, the ratio of PCs affected by the hot-spot over the non-affected ones becomes very small with a consequent reduction of the $T^2(m,n)$ sensitivity. The threshold at 80% reduces the performances of the ST-PCA based approach as well, but at a lower extent. When the recursive update is used, the hot-spot is always detected by using the ST-PCA, although after a longer duration. When the moving window update is used, instead, the ST-PCA based approach is able to detect only a hot-spot of medium or large dimensions. This is caused by the fact that a window size $L = 50$ is too small for the lowest severity out-of-control condition: a larger window size or a recursive technique would be needed.

Regarding the different spatial weight definitions, Table 3 shows that the weights W_1, W_2 and W_3 provide analogous results, which highlights the robustness of the ST-PCA-based method with respect to how spatial weights are defined.

5. Experimental results

5.1. Comparison study

The proposed approach was compared against two alternative methods described in Grasso *et al*. (2017). The first competitor represents the most intuitive and simplest method to detect out-of-control states in video images. It consists of monitoring directly the average pixel intensities of the image stream. For each pixel, the mean intensity over the J observed frames is computed, $\overline{\boldsymbol{U}} = \{\overline{\boldsymbol{u}}_{m,n} = (1/J)\sum_j u_{m,n,j}\}$, and the

clustering-based alarm rule is applied to $\bar{\boldsymbol{U}}$. The second competitor is the simple T-mode PCA-based approach. All the methods were tested by using either the recursive or the moving window updating scheme. In this latter case, a default length of the moving window $L = 50$ was considered, but the results of a sensitivity analysis with respect to this parameter are discussed in sub-section 5.2. The T-mode PCA and ST-PCA were compared by retaining the number m of PCs that captured at least 80% of the overall variability.

Fig. 16, Fig. 17 and Fig. 18 show the results of the T-mode PCA and ST-PCA based methods for the three OOC scenarios, when the recursive updating scheme was used. In particular, they show the estimated T^2 statistic when a hot-spot alarm signal was issued. Although the $T^2(m,n)$ values from different PCA formulations belong to different scales, the colormap on the left and central panels was set in order to keep a similar range of colours. The right panels of Fig 16, 17 and 18, instead, use black, grey and red colours to represent the background, normal melting and hot-spot areas (when detected), respectively.

The overall results of all the compared methods are eventually shown in Table 4. Additional information about the dataset and the nature of the signalled events are discussed in Appendix A.

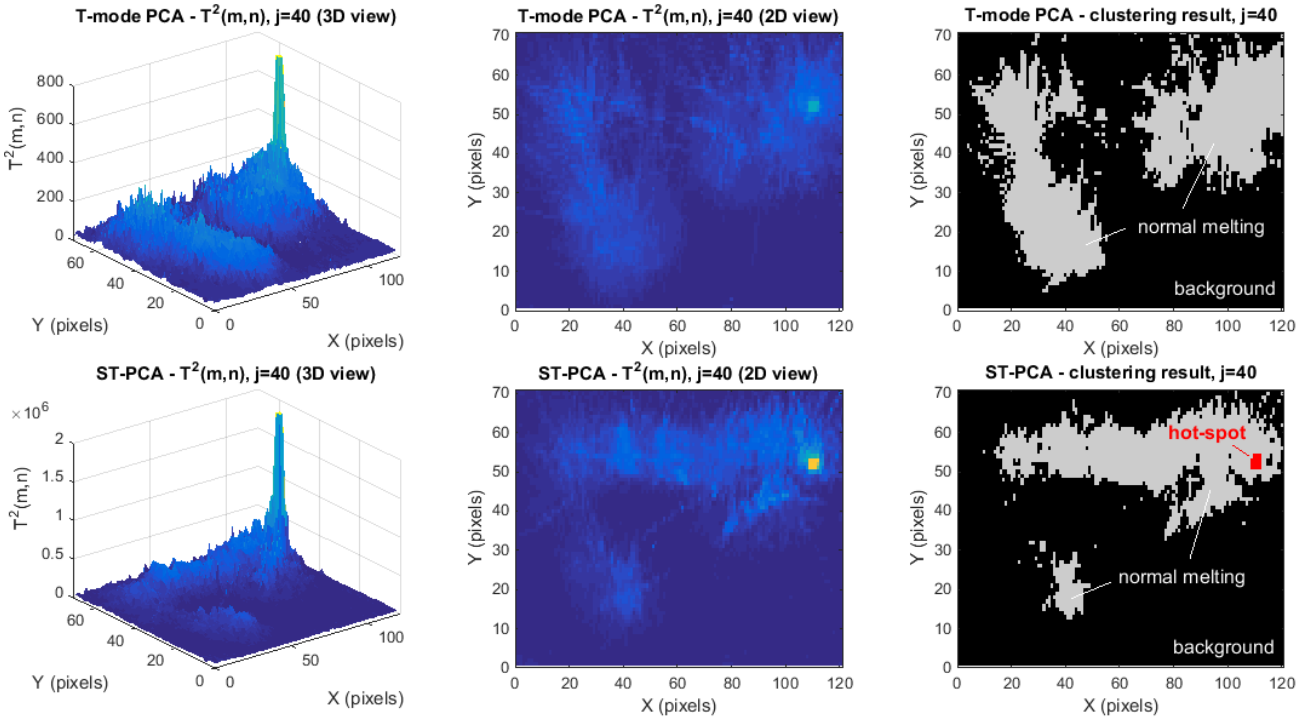

FIGURE 16 – Results of T-mode and ST-PCA based methods with recursive updating in OOC scenario 1, $j = 40$ (first hot-spot detection)

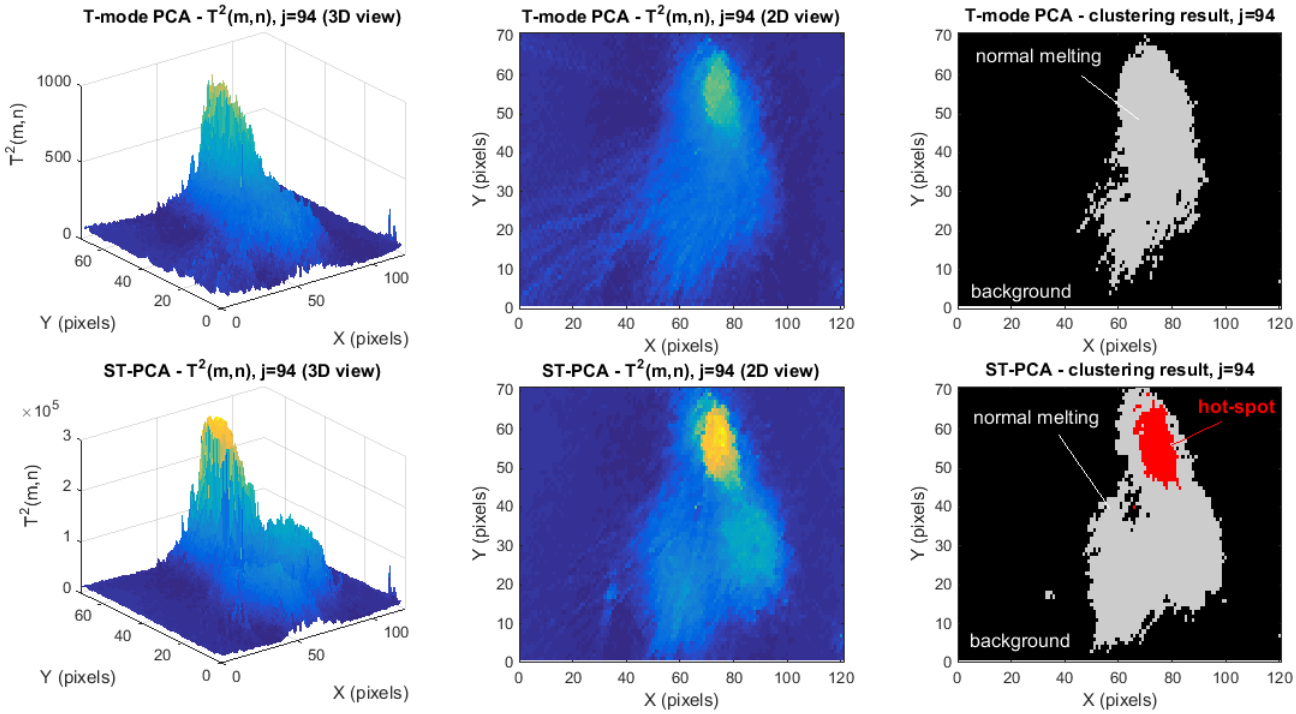

FIGURE 17 – Results of T-mode and ST-PCA based methods with recursive updating in OOC scenario 2, $j = 94$ (first hot-spot detection)

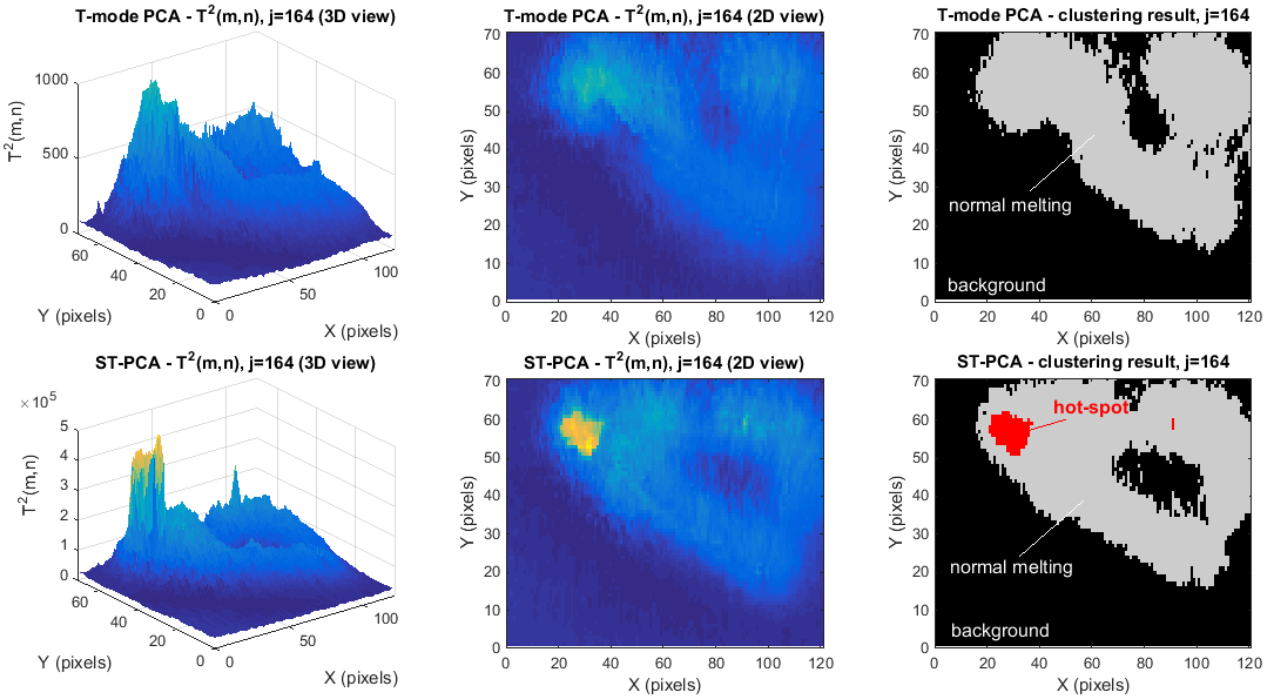

FIGURE 18 – Results of T-mode and ST-PCA based methods with recursive updating in OOC scenario 3, $j = 164$ (first hot-spot detection)

TABLE 4 – Results of compared methods in the IC scenario and OOC scenarios 1, 2 and 3

Approach		Time of first signal (frame index)	Signalled defect area (# pixels)	Signalled defect location (X) (pixels)	Signalled defect location (Y) (pixels)
OOC Scenario 1					
Average intensity	Recursive	*No detection*	-	-	-
	Mov. window	*No detection*	-	-	-
T-mode PCA	Recursive	$j = 201$	79	106.27	52.28
	Mov. window	$j = 198$	101	104.25	52.71
ST-PCA	Recursive	$\boldsymbol{j = 40}$	15	110.60	52.40
	Mov. window	$\boldsymbol{j = 40}$	15	110.60	52.40
OOC Scenario 2					
Average intensity	Recursive	$j = 144$	193	74.86	53.81
	Mov. window	*No detection*	-	-	-
T-mode PCA	Recursive	$j = 95$	219	74.95	54.49
	Mov. window	*No detection*	-	-	-
ST-PCA	Recursive	$j = 94$	231	74.29	55.80
	Mov. window	$\boldsymbol{j = 92}$	243	74.81	55.98
OOC Scenario 3					
Average intensity	Recursive	*No detection*	-	-	-
	Mov. window	$j = 173$	273	33.88	55.73
T-mode PCA	Recursive	$j = 169$	482	41.90	56.59
	Mov. window	$j = 168$	151	31.19	56.25
ST-PCA	Recursive	$j = 164$	131	30.31	56.94
	Mov. window	$\boldsymbol{j = 153}$	168	29.21	55.75

In OOC scenario 1 (Fig. 16), the first alarm was signalled at frame $j = 40$ by the ST-PCA based approach, in correspondence of a first short-duration hot-spot occurrence in the defective acute corner of the triangular shape. In the same scenario, the T-mode PCA yields a local peak of the $T^2(m,n)$, but it is not sufficient to signal an alarm by means of the clustering-based rule. Indeed, the T-mode PCA based approach allows signalling the hot-spot only at frame $j = 201$ (when the recursive update is used), i.e., when the hot-spot becomes much more severe in terms of both size and duration (see also Appendix A). The improved performances provided by the ST-PCA result from a better characterization of both the spatial and temporal correlation of pixel intensity profiles. In correspondence of the hot-spot, even when it is limited in size and intensity, the ST-PCA inflates the local peak of the $T^2(m,n)$ statistic by taking into account the spatial closeness of the pixels within the defective region, which enhances the capability of signalling that region as an additional cluster. In OOC scenarios 2 and 3 (Fig. 17 and Fig. 18), the hot-spot covers a larger area but, at least at the beginning of the process, its duration is too short for an early detection. However, the ST-PCA yields a faster detection also in these two additional scenarios, even if the gap between the performances of the methods based on the two PCA variants is smaller than in scenario 1. Table 4 summarizes the performances of all the compared methods in terms of i) time of first detection, ii) area of the signalled OOC cluster and iii) coordinates of its centroid.

The latter two information allows one to compare the results not only in terms of time to signal, but also in terms of hot-spot localization (centroid coordinates) and size.

The simple method based on monitoring the average pixel intensities is the less effective one, as it is not able to signal the hot-spot in some cases, or, in other cases, it yields the larger detection delay among the compared methods. The ST-PCA based approach outperforms the two competitors thanks to an anticipated defect detection capability in OOC scenario 1. In scenario 2, the T-mode PCA is able to signal the hot-spot only when coupled with a recursive updating scheme. In scenario 3, the T-mode PCA based approach with recursive update signals a defective area that is more elongated along the X direction than the actual hot-spot. This is caused by the worst hot-spot localization provided by the corresponding $T^2(m,n)$ statistic compared with the same statistic originated by the ST-PCA in the same scenario (see Fig. 18).

Generally speaking, the ST-PCA based approach is not only faster in detecting the defect, but it is also the only method that leads to an alarm in all the considered OOC scenarios, regardless of the iterative updating scheme. The recursive and the moving window ($L = 50$) updating methods, coupled with the ST-PCA, provide quite similar performances. A sensitivity analysis with respect to the parameter L is discussed in the following sub-section.

5.2. Sensitivity analysis

Table 4 showed that the moving window updating scheme with window length $L = 50$ is not only more computationally efficient but also comparable to the recursive approach in terms of defect detection power. However, the performances may be influenced by the choice of the parameter L. A sensitivity analysis was performed to investigate this effect. The moving window ST-PCA based approach was tested with different window lengths and the results are summarized in Table 5.

In all the considered cases, the results are quite robust to the choice of the parameter L, as the hot-spot is detected with similar delays and no false alarms are produced even in the presence of small values of L. Generally speaking, small moving window lengths may filter out longer process dynamics with detrimental effects on the characterization of the temporal auto-correlation of pixel profiles. On the other hand, large moving window lengths provide no computational benefit against the recursive updating scheme. Thus, a trade off between these two effects should drive the selection of the parameter L, from a practical implementation viewpoint.

TABLE 5 – Sensitivity of the proposed ST-PCA based approach to the moving window length in OOC scenario 1, 2 and 3

Size of moving window (L)	Time of first signal (frame index)	Signalled defect area (# pixels)	Signalled defect location (X) (pixels)	Signalled defect location (Y) (pixels)
OOC scenario 1				
20	$j = 40$	11	110.36	52.10
30	$j = 40$	12	110.50	52.00
50	$j = 40$	15	110.60	52.40
70	$j = 40$	15	110.60	52.40
OOC Scenario 2				
20	$j = 88$	174	74.25	56.31
30	$j = 89$	180	74.55	56.24
50	$j = 92$	243	74.81	55.98
70	$j = 92$	243	74.33	55.62
OOC Scenario 3				
20	$j = 166$	204	27.33	57.03
30	$j = 152$	197	27.71	56.53
50	$j = 153$	168	29.21	55.75
70	$j = 168$	156	29.21	56.33

5.3. Computational costs and implementation guidelines

Both the T-mode PCA and ST-PCA required about $0.15 \div 0.30\ s$ on a computer equipped with an Intel® Core™ i7-3537 CPU @ 2.00 GHz when the data matrix encloses all the 320 frames of size 121×71 pixels (OOC scenarios). If the number of frames included into the processed data matrix is kept fixed (moving window approach), the overall computation time can be strongly reduced, e.g. less than $0.06\ s$ with $L = 50$. More efficient implementations for real-time use are expected to yield a further consistent reduction of the required time. Future research will be aimed at evaluating applications and possible extensions with larger images sizes for in-situ monitoring of wider areas of the build.

Based on the outcome of the sensitivity analysis previously discussed, and on computational efficiency considerations, the following practical implementation guidelines can be advocated:

- The ST-PCA analysis should be initialized with a sufficient number of frames, i.e., the first ST-PCA model should include at least $40 - 50$ frames since the beginning of the process. This may reduce the

risk of false alarms caused by an over-fitting to few initial observations.

- The recursive updating scheme can be used at the beginning of the process to iteratively augment the data matrix up to a sufficient dimension, L, to properly characterize the process dynamics. Then, the moving window updating scheme can be used to keep fixed the size L of the matrix and the computational cost.
- If the updating of the ST-PCA model and clustering analysis for each single frame is not computationally feasible, it is possible to apply a batch-wise update: the PCA model is updated only when a new batch of B frames has been made available, where B should be chosen depending on computational contraints. However, it is worth noticing that the larger is B, the lower is the potential reactivity of the defect detection method.

6. Conclusion

The increasing use of machine vision systems in advanced manufacturing applications is reshaping the nature of process data in SPM applications, leading to the adoption of novel big data perspectives. Indeed, machine vision pushes the need for image-based statistical process monitoring methods able to deal with large amounts of data characterized by new formats (i.e., images or video images) acquired at high speed (possibly up to thousands of frames per second). In this framework, one goal of industrial interest consists of determining both when and where a defect originated during the monitored process via video image analysis. To this aim, we proposed a novel approach based on spatially weighted PCA aimed at representing the spatio-temporal signature of the process enclosed in the monitored video image data. The simulation analysis showed that this approach is more effective than the basic T-mode PCA formulation in detecting the onset of a local defect. A real case study in metal additive manufacturing was proposed. This represents one of the most recent industrial applications of machine vision systems, where in-situ cameras could be used to monitor the stability of the process and to detect and localise defects during the layer-wise production of the part. Nevertheless, the mainstream literature and commercially available systems still lack automated defect detection capabilities. The ST-PCA technique was coupled with a k-means clustering-based alarm rule that exploits engineering knowledge about the process, without the need for a training phase. The experimental results showed that the proposed approach allows identifying hot-spots caused by out-of-control overheating phenomena faster than competitor methods.

Future research could be aimed at tuning and extending the method to make it applicable in real time for continuous process monitoring. A relevant extension of the present study regards the development of novel control charting methods based on continuous statistics, with an enhanced capability of controlling the Type I error performances. Further analysis may also address the extendibility of the method to other types of detect and other image acquisition setups.

References

Armingol JM, Otamendi J, de la Escalera A, Pastor JM, Rodriguez FJ (2003). Statistical pattern modeling in vision-based quality control systems. Journal of Intelligent and Robotic Systems; 37:321 – 336.

Bharati, M. H., & MacGregor, J. F. (1998). Multivariate image analysis for real-time process monitoring and control. Industrial & Engineering Chemistry Research, 37(12), 4715-4724.

Bharati, M. H., MacGregor, J. F., & Tropper, W. (2003). Softwood lumber grading through on-line multivariate image analysis techniques. Industrial & Engineering Chemistry Research, 42(21), 5345-5353.

Bui, A. T., & Apley, D. W. (2017). A monitoring and diagnostic approach for stochastic textured surfaces. Technometrics, (in press).

Compagnucci, R. H., Araneo, D., & Canziani, P. O. (2001). Principal sequence pattern analysis: a new approach to classifying the evolution of atmospheric systems. International journal of climatology, 21(2), 197-217.

De Ketelaere, B., Hubert, M., & Schmitt, E. (2015). Overview of PCA-Based Statistical Process-Monitoring Methods for Time-Dependent, High-Dimensional Data. Journal of Quality Technology, 47(4), 318.

Demšar, U., Harris, P., Brunsdon, C., Fotheringham, A. S., & McLoone, S. (2013). Principal component analysis on spatial data: an overview. Annals of the Association of American Geographers, 103(1), 106-128.

Everton, S. K., Hirsch, M., Stravroulakis, P., Leach, R. K., & Clare, A. T. (2016). Review of in-situ process monitoring and in-situ metrology for metal additive manufacturing. Materials & Design, 95, 431-445.

Funck, J. W., Zhong, Y., Butler, D. A., Brunner, C. C., & Forrer, J. B. (2003). Image segmentation algorithms applied to wood defect detection. Computers and electronics in agriculture, 41(1), 157-179.

Gallagher, N., Wise, B., Butler, S., White, D., and Barna, G. (1997). "Development and Benchmarking of Multivariate Statistical Process Control Tools for a Semiconductor Etch Process: Improving Robustness through Model Updating". Process: Impact of

Measurement Selection and Data Treatment on Sensitivity, Safe process 97, pp. 26–27.
Geladi, P., & Grahn, H. F. (1996). Multivariate image analysis. John Wiley & Sons, Ltd.
Gibson, I., Rosen, D. W., Stucker, B. 2010. "Additive manufacturing technologies". New York: Springer.
Gollini I, Lu B, Charlton M, Brunsdon C, Harris P (2015), GWmodel: an R Package for exploring Spatial Heterogeneity using Geographically Weighted Models. Journal of Statistical Software 63(17): 1-50
Graham, K. J., Krishnapisharody, K., Irons, G. A., & MacGregor, J. F. (2007). Ladle eye area measurement using multivariate image analysis. Canadian Metallurgical Quarterly, 46(4), 397-405.
Grasso, M., & Colosimo, B. M. (2017). Process defects and in situ monitoring methods in metal powder bed fusion: a review. Measurement Science and Technology, 28(4), 044005.
Grasso, M., Laguzza, V., Semeraro, Q., & Colosimo, B. M. (2017). In-Process Monitoring of Selective Laser Melting: Spatial Detection of Defects Via Image Data Analysis. Journal of Manufacturing Science and Engineering, 139(5), 051001.
Grasso M., Colosimo B.M., Pacella M. (2014), Profile Monitoring via Sensor Fusion: the use of PCA Methods for Multi-Channel Data, International Journal of Production Research, 52 (20), 6110 – 6135
Harris, P., Brunsdon, C., Charlton, M., Juggins, S., & Clarke, A. (2014). Multivariate spatial outlier detection using robust geographically weighted methods. Mathematical Geosciences, 46(1), 1-31.
Harris P, Brunsdon C, Charlton M (2011) Geographically weighted principal components analysis. Int J Geogr Inf Sci 25:1717–1736
Harris P, Clarke A, Juggins S, Brunsdon C, Charlton M (2015) Enhancements to a geographically weighted principal components analysis in the context of an application to an environmental data set. Geographical Analysis 47: 146-172
Hastie, T., Tibshirani, R., & Friedman, J. (2009). Unsupervised learning. In The elements of statistical learning (pp. 485-585). Springer New York.
He, Z., Zuo, L., Zhang, M., & Megahed, F. M. (2016). An image-based multivariate generalized likelihood ratio control chart for detecting and diagnosing multiple faults in manufactured products. International Journal of Production Research, 54(6), 1771-1784.
Horst, R. L., & Negin, M. (1992). Vision system for high-resolution dimensional measurements and on-line SPC: web process application. IEEE transactions on industry applications, 28(4), 993-997.
Jiang BC, Wang C-C, Liu H-C. (2005) Liquid crystal display surface uniformity defect inspection using analysis of variance and exponentially weighted moving average techniques. International Journal of Production Research; 43:67 – 80.
Jiang, B. C., & Jiang, S. J. (1998). Machine vision based inspection of oil seals. Journal of manufacturing systems, 17(3), 159-166.
Jolliffe, I. (2002). Principal component analysis. John Wiley & Sons, Ltd.
Jombart, T., Devillard, S., Dufour, A.-B. & Pontier, D. (2008) Revealing cryptic spatial patterns in genetic variability by a new multivariate method, Heredity, 101, 92 – 103.
Koren, Y., & Carmel, L. (2004). Robust linear dimensionality reduction. IEEE transactions on visualization and computer graphics, 10(4), 459-470.
Li, W., Yue, H. H., Valle-Cervantes, S., & Qin, S. J. (2000). Recursive PCA for adaptive process monitoring. Journal of process control, 10(5), 471-486.
Liang, Y. T., & Chiou, Y. C. (2008, June). Vision-based automatic tool wear monitoring system. In Intelligent Control and Automation, 2008. WCICA 2008. 7th World Congress on (pp. 6031-6035). IEEE.
Lin, H. D., & Chiu, S. W. (2006, December). Computer-aided vision system for MURA-type defect inspection in liquid crystal displays. In Pacific-Rim Symposium on Image and Video Technology (pp. 442-452). Springer Berlin Heidelberg.
Lin, H. D. (2007a). Automated visual inspection of ripple defects using wavelet characteristic based multivariate statistical approach. Image and Vision Computing, 25(11), 1785-1801.
Lin, H. D. (2007b). Computer-aided visual inspection of surface defects in ceramic capacitor chips. Journal of Materials Processing Technology, 189(1), 19-25.
Lin, H. D., Chung, C. Y., & Lin, W. T. (2008). Principal component analysis based on wavelet characteristics applied to automated surface defect inspection. WSEAS Transactions on Computer Research, 3(4), 193-202.
Lu C-J, Tsai D-M. (2005) Automatic defect inspection for LCDs using singular value decomposition. The International Journal of Advanced Manufacturing Technology; 25:53 – 61.
Lu H., Plataniotis K.N., Venetsanopoulos A.N., (2008a) MPCA: Multilinear principal component analysis of tensor objects, IEEE Trans.Neural Netw., 19(1), 18–39.
Lu H., Plataniotis K.N., Venetsanopoulos A.N., (2008b) Uncorrelated multilinear principal component analysis through successive variance maximization, in Proc. 25th Int. Conf. Mach. Learn., 616–623.
Lyu, J., & Chen, M. (2009). Automated visual inspection expert system for multivariate statistical process control chart. Expert Systems with Applications, 36(3), 5113-5118.
MacGregor, J. F., Bharati, M. H., & Yu, H. (2001, February). Multivariate image analysis for process monitoring and control. In Intelligent Systems and Smart Manufacturing (pp. 17-26). International Society for Optics and Photonics.
Mani, M., Lane, B., Donmez, A., Feng, S., Moylan, S., & Fesperman, R. (2015). Measurement science needs for real-time control of additive manufacturing powder bed fusion processes. National Institute of Standards and Technology, Gaithersburg, MD, NIST Interagency/Internal Report (NISTIR), 8036.
Megahed, F. M., & Jones-Farmer, L. A. (2015). Statistical Perspectives on "Big Data". In Frontiers in Statistical

Quality Control 11 (pp. 29-47). Springer International Publishing.
Megahed, F. M., Woodall, W. H., & Camelio, J. A. (2011). A review and perspective on control charting with image data. Journal of Quality Technology, 43(2), 83.
Megahed, F. M., Wells, L. J., Camelio, J. A., & Woodall, W. H. (2012). A spatiotemporal method for the monitoring of image data. Quality and Reliability Engineering International, 28(8), 967-980.
Nembhard, H. B., Ferrier, N. J., Osswald, T. A., & Sanz-Uribe, J. R. (2003). An integrated model for statistical and vision monitoring in manufacturing transitions. Quality and Reliability Engineering International, 19(6), 461-476.
Park, C., Huang, J. Z., Huitink, D., Kundu, S., Mallick, B. K., Liang, H., and Ding, Y. (2012). A multistage, semi-automated procedure for analyzing the morphology of nanoparticles. IIE Transactions, 44(7):507–522.
Park, C., & Shrivastava, A. K. (2014). Multimode geometric-profile monitoring with correlated image data and its application to nanoparticle self-assembly processes. Journal of Quality Technology, 46(3), 216.
Qiu, P. (2005). Image processing and jump regression analysis (Vol. 599). John Wiley & Sons.
Qiu, P. (2017). Statistical Process Control Charts as a Tool for Analyzing Big Data. In Big and Complex Data Analysis (pp. 123-138). Springer International Publishing.
Qiu, P. and Yandell, B. (1997). Jump detection in regression surfaces. Journal of Computational and Graphical Statistics, 6(3):332–354.
Qiu, P. and Sun, J. (2007). Local smoothing image segmentation for spotted microarray images. Journal of the American Statistical Association, 102(480):1129–1144.
Qin, S. J. (2014). Process data analytics in the era of big data. AIChE Journal, 60(9), 3092-3100.
Schölkopf, B., Smola, A., & Müller, K. R. (1997, October). Kernel principal component analysis. In International Conference on Artificial Neural Networks, 583-588, Springer, Berlin, Heidelberg.
Spears, T. G., & Gold, S. A. (2016). In-process sensing in selective laser melting (SLM) additive manufacturing. Integrating Materials and Manufacturing Innovation, 5(1), 1.
Stahlschmidt, S., Härdle, W. K., & Thome, H. (2015). An application of principal component analysis on multivariate time-stationary spatio-temporal data. Spatial Economic Analysis, 10(2), 160-180.
Tan, J., Chang, Z., & Hsieh, F. (1996). Implementation of an automated real-time statistical process controller. Journal of food process engineering, 19(1), 49-61.
Tapia, G., & Elwany, A. (2014). A review on process monitoring and control in metal-based additive manufacturing. Journal of Manufacturing Science and Engineering, 136(6), 060801.
Tong, L. I., Wang, C. H., & Huang, C. L. (2005). Monitoring defects in IC fabrication using a Hotelling T/sup 2/control chart. IEEE transactions on semiconductor manufacturing, 18(1), 140-147.
Tsutsumida N, Harris P, Comber A (2017) The application of a geographically weighted principal components analysis for exploring 23 years of goat population change across Mongolia. Annals of the Association of American Geographers.107(5): 1060-1074
Tunák, M., & Linka, A. (2008). Directional defects in fabrics. Research Journal of Textile and Apparel, 12(2), 13-22.
Tunák, M., Linka, A., & Volf, P. (2009). Automatic assessing and monitoring of weaving density. Fibers and Polymers, 10(6), 830-836.
Wang, X., Kruger, U., & Irwin, G. W. (2005). Process monitoring approach using fast moving window PCA. Industrial & Engineering Chemistry Research, 44(15), 5691-5702.
Wang, K., & Tsung, F. (2005). Using profile monitoring techniques for a data-rich environment with huge sample size. Quality and reliability engineering international, 21(7), 677-688.
Wartenberg, D. (1985). Multivariate spatial correlation: a method for exploratory geographical analysis. Geographical Analysis, 17(4), 263-283.
Wold, S. (1994). "Exponentially Weighted Moving Principal Components Analysis and Projections to Latent Structures". Chemometrics and Intelligent Laboratory Systems, 23(1), pp. 149–161.
Yan, H., Paynabar, K., & Shi, J. (2015). Image-based process monitoring using low-rank tensor decomposition. IEEE Transactions on Automation Science and Engineering, 12(1), 216-227.
Yan, H., Paynabar, K., & Shi, J. (2017). Anomaly detection in images with smooth background via smooth-sparse decomposition. Technometrics, 59(1), 102-114.
Yu, H., & MacGregor, J. F. (2004). Monitoring flames in an industrial boiler using multivariate image analysis. AIChE Journal, 50(7), 1474-1483.
Zhao, Q., Xu, M., Fränti, P., 2009, "Sum-of-squares based cluster validity index and significance analysis. Adaptive and Natural Computing Algorithms", Lecture Notes in Computer Science, 5495, pp. 313-322
Zhang, Z. 2000 "A Flexible New Technique for Camera Calibration". IEEE Transactions on Pattern Analysis and Machine Intelligence. 22(11), 1330–1334.

Appendix A

Fig. A1, A2 and A3 show some examples of frames belonging respectively to OOC scenario 1, 2 and 3. The red arrow indicates the location of the hot-pot detected by the proposed approach.

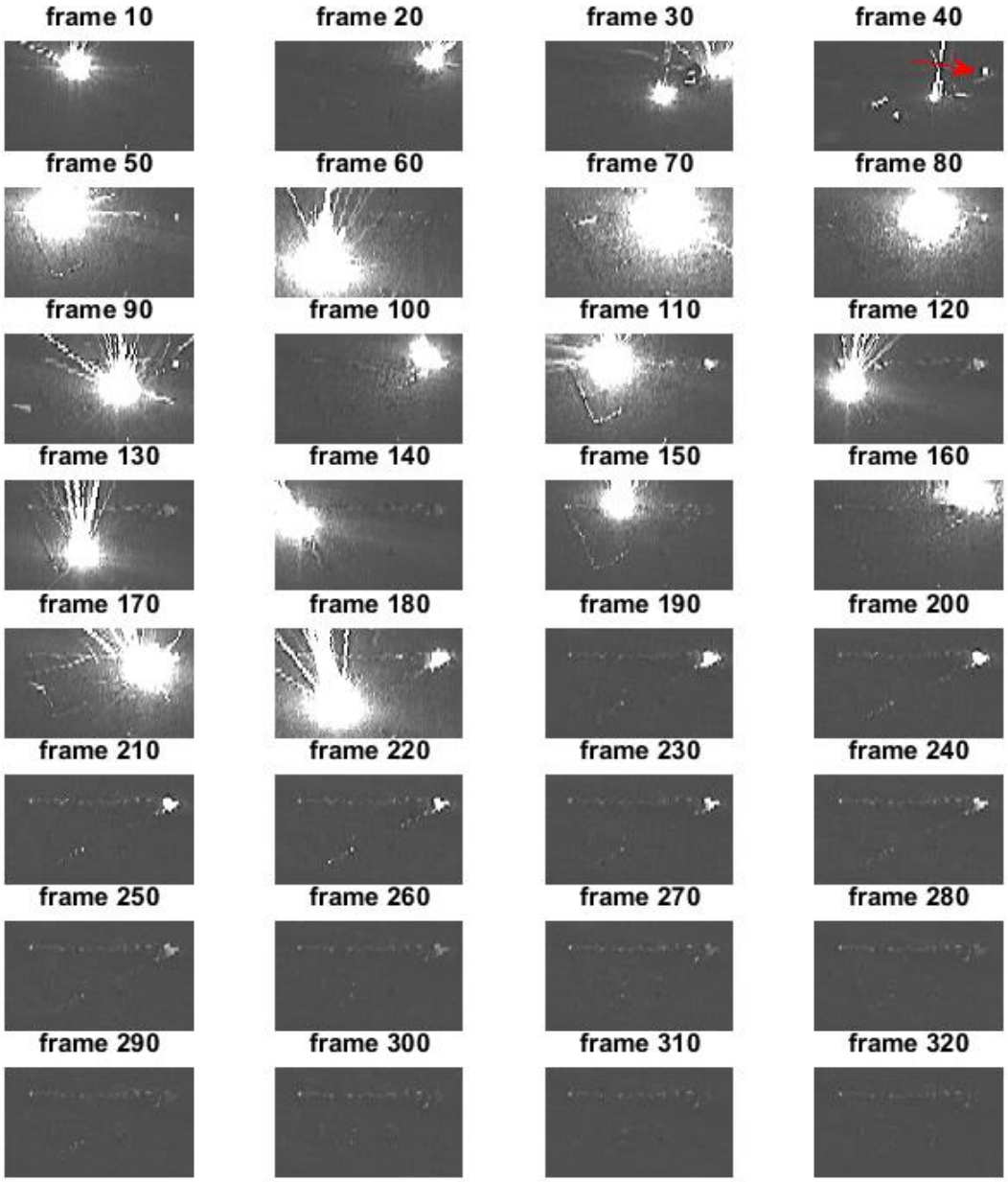

FIGURE A1 – Example of frames belonging to the video image dataset corresponding to OOC scenario 1

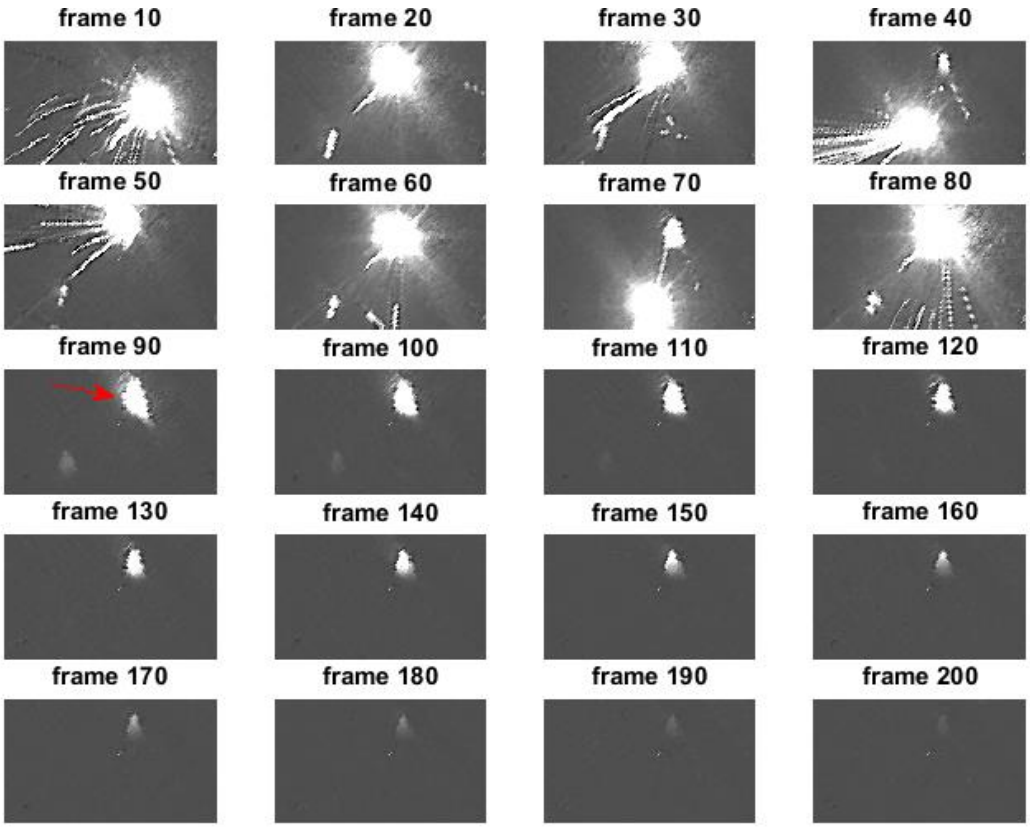

FIGURE A2 – Example of frames belonging to the video image dataset corresponding to OOC scenario 2

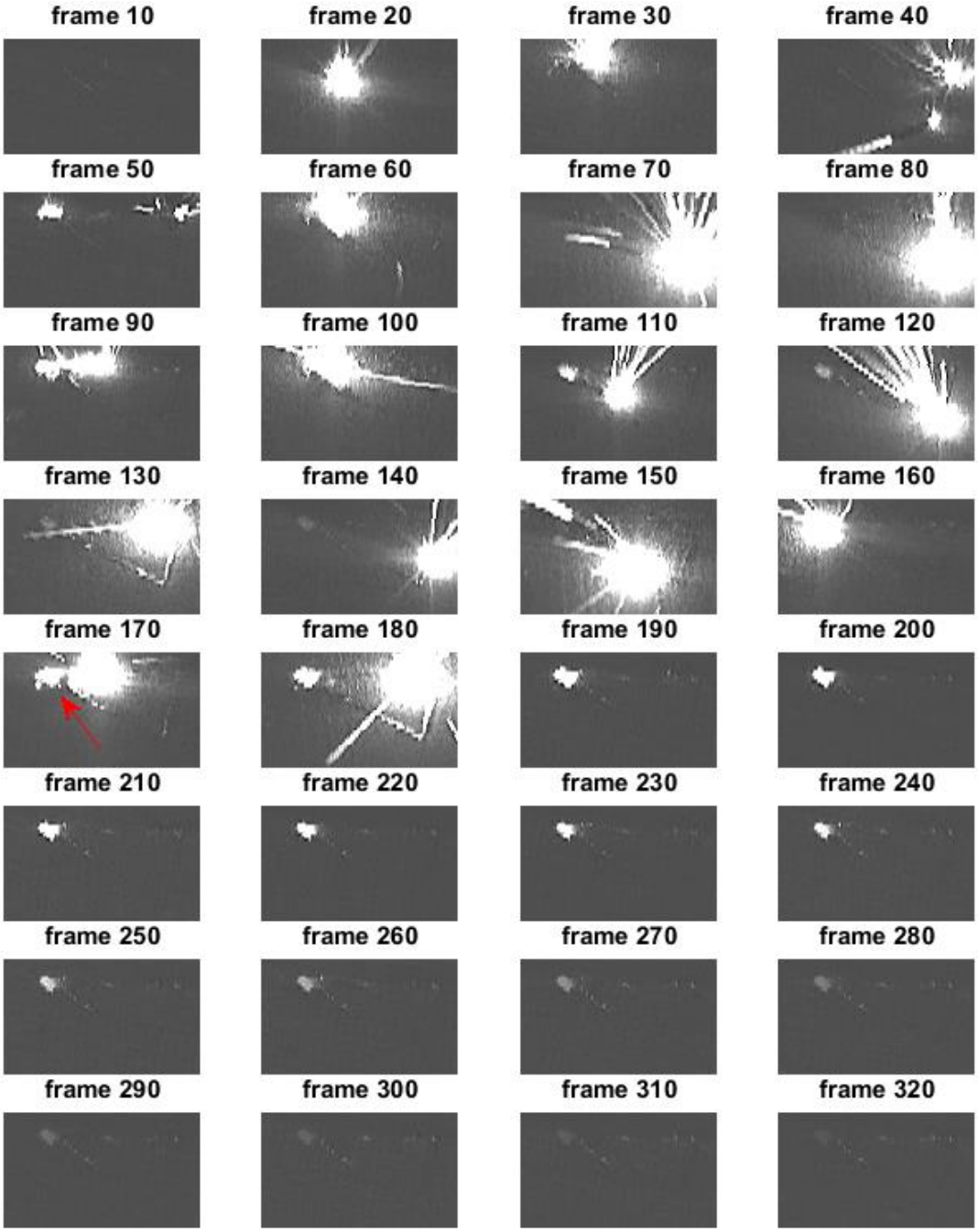

FIGURE A3 – Example of frames belonging to the video image dataset corresponding to OOC scenario 3